NASA Contractor Report 181671

ICASE REPORT NO. 88-33

ICASE

SPATIAL STABILITY OF A COMPRESSIBLE MIXING LAYER

T. L. Jackson

C. E. Grosch

Contract No. NAS1-18107
June 1988

INSTITUTE FOR COMPUTER APPLICATIONS IN SCIENCE AND ENGINEERING
NASA Langley Research Center, Hampton, Virginia 23665

Operated by the Universities Space Research Association

National Aeronautics and
Space Administration

Langley Research Center
Hampton, Virginia 23665

SPATIAL STABILITY OF A COMPRESSIBLE MIXING LAYER

T. L. Jackson

Department of Mathematical Sciences
Old Dominion University
Norfolk, Virginia 23529

C. E. Grosch

Department of Oceanography and
Department of Computer Science
Old Dominion University
Norfolk, Virginia 23529

Abstract. We present the results of a study of the inviscid spatial stability of a parallel compressible mixing layer. The parameters of this study are the Mach number of the moving stream, the ratio of the temperature of the stationary stream to that of the moving stream, the frequency and the direction of propagation of the disturbance wave. Stability characteristics of the flow as a function of these parameters are given. It is shown that if the Mach number exceeds a critical value there are always two groups of unstable waves. One of these groups is fast with phase speeds greater than 1/2, and the other is slow with phase speeds less than 1/2. Phase speeds for the neutral and unstable modes are given, as well as growth rates for the unstable modes. It is shown that three dimensional modes have the same general behavior as the two dimensional modes but with higher growth rates over some range of propagation direction. Finally, we have found for sufficiently large Mach numbers a group of very low frequency unstable modes. These modes have very low phase speeds but large growth rates.

This work was supported under the National Aeronautics and Space Administration under NASA Contract NAS1-18107 while the authors were in residence at the Institute for Computer Applications in Science and Engineering, NASA Langley Research Center, Hampton, VA 23665.

1. Introduction. An understanding of the stability characteristics of compressible mixing layers is of fundamental interest and is also extremely important in view of the projected use of the scramjet engine for the propulsion of hypersonic aircraft. Knowledge of these characteristics may allow one, in principle, to control the downstream evolution of such flows. This is particularly important because of the observed increase in the flow stability at high Mach numbers (Papamoschou and Roshko, 1986). Because of the gain in stability, natural transition may occur at downstream distances which are larger than practical combustor lengths. A number of techniques to enhance mixing are discussed by Kumar, Bushnell, and Hussaini (1987). A detailed understanding of the linear stability characteristics of compressible mixing layers will be of aid in mixing enhancement.

In this paper we will examine the inviscid stability of a compressible mixing layer, the interfacial region between a moving gas at $+\infty$ and a stationary gas at $-\infty$. The stability of the mixing layer in a compressible fluid has not been studied as extensively as the same flow in an incompressible fluid. The basic formulation of the theory for the stability of compressible shear flows, both free and wall bounded, is due to Lees and Lin (1946), and Dunn and Lin (1955) first showed the importance of three dimensional disturbances for the stability of these flows.

The inviscid temporal stability of the compressible mixing layer to two and three dimensional disturbances was studied by Lessen, Fox and Zien for subsonic disturbances (1965) and supersonic disturbances (1966). Lessen et al. assumed that the flow was iso-energetic and, as a consequence, the temperature in the stationary gas was always greater than that of the moving gas. In fact, because the ratio of the temperatures at $\pm\infty$ varies as the square of the Mach number, the stationary gas is much hotter than the moving gas at even moderatly supersonic speeds.

Gropengiesser (1969) reexamined this problem, but without using the iso-energetic assumption. Consequentally, he was able to treat the ratio of the temperatures of the stationary and moving gas as a parameter. He carried out inviscid spatial stability calculations for the compressible mixing layer for a temperature ratio of 0.6, 1.0 and 2.0 and for Mach numbers between 0 and 3. We will discuss Gropengiesser's results in comparison with ours in a later section.

The results reported here were obtained as the first part of a study of the stability of compressible mixing layers in which a diffusion flame is embedded (Jackson and Hussaini, 1988). We are primarily interested in solving the stability problem in the high Mach number regime. As will be seen below, it appears necessary to only consider the range $0 \leq M \leq 10$ in order to be able to deduce the asymptotic ($M \rightarrow \infty$) structure of the solutions. In order to understand the effect of the heat release on the stability of this flow, one must first understand the stability characteristics of a nonreacting flow. It is well known (see Mack (1984) for example) that the inviscid theory is a reliable guide for understanding the stability of compressible shear flows at moderate and large Reynolds numbers. Thus we consider only the inviscid spatial stability problem.

We began this study by taking the mean velocity profile in the mixing layer to be that of the Lock profile (Lock, 1951). In the course of carrying out the stability calculations for this profile with different sets of values of the basic parameters, we noted some quite interesting features of the solutions, particularly at higher Mach numbers. In order to examine these features in more detail, we replaced the Lock profile with a hyperbolic tangent profile. This is a reasonable

approximation to the Lock profile and has been used by many investigators in studying the stability of incompressible mixing layers, see Michalke (1972), Monkewitz and Huerre (1982), and Ho and Huerre (1984) and references contained therein. More importantly from our point of view, we can obtain certain results analytically if we use the hyperbolic tanget profile to approximate the velocity distribution in the mixing layer. Results for the Lock profile will be presented at a later date.

In section 2 we give the basic equations governing the mean flow and the small amplitude disturbance equations. The boundary condition and the numerical method are also discussed in this section. Section 3 contains a presentation of our results and conclusions are given in section 4.

2. Formulation of the Problem. We consider the stability of a compressible mixing layer, with zero pressure gradient, which separates two streams of different speeds and temperatures. We assume that the mean flow is governed by the compressible boundary layer equations (Stewartson, 1964). The x-axis is taken along the direction of the flow, the y-axis normal to the flow, and the z-axis in the cross-stream direction. We let (U,V,0) be the velocity and T the temperature of this mean flow. All of the variables are nondimensionalized using the freestream values at $y = +\infty$. In what follows we assume that the Prandtl number is unity.

The mean flow equations are first transformed into the incompressible form by means of the Howarth-Dorodnitzyn transformation

$$Y = \int_0^y \rho \, dy, \quad \hat{V} = \rho V + U \int_0^y \rho_x \, dy, \tag{2.1}$$

where ρ is the density and, because the pressure gradient is zero,

$$\rho T = 1. \tag{2.2}$$

Next we transform to the similarity variable

$$\eta = \frac{Y}{2\sqrt{xC}}, \tag{2.3}$$

where C is the constant in Chapman's (1950) linear viscosity law

$$\mu = CT. \tag{2.4}$$

These equations have as a solution the similarity solution given by Lock (1951). However, as discussed in the introduction, we assume here that

$$U = \frac{1}{2}\,(1 + tanh(\eta)), \tag{2.5}$$

which approximates the Lock profile and can be handled analytically. This profile also satisfies the boundary conditions

$$U \to 1 \quad as \quad y \to +\infty, \qquad U \to 0 \quad as \quad y \to -\infty. \tag{2.6}$$

As is well known, the temperature distribution can be expressed in terms of the velocity field. The temperature boundary conditions are

$$T \to 1 \quad as \quad y \to +\infty, \qquad T \to \beta_T \quad as \quad y \to -\infty. \tag{2.7}$$

This yields

$$T = 1 - (1-\beta_T)(1-U) + \frac{\gamma-1}{2} M^2 U (1-U), \tag{2.8}$$

where γ is the ratio of specific heats and M is the Mach number at $+\infty$. If β_T is less than one, the stationary gas is relatively cold compared to the moving stream, and if β_T is greater than one it is relatively hot.

The flow field is perturbed by introducing wave disturbances in the velocity, pressure, temperature and density with amplitudes which are functions of η. For example, the pressure perturbation is

$$p = \Pi(\eta)\, exp[i(\alpha x + \beta z - \omega t)], \tag{2.9}$$

with Π the amplitude, α and β the wavenumbers in the downstream (x) and cross-stream (z) directions, respectively, and ω the frequency which is taken to be real. As mentioned in the introduction, we are only treating the spatial stability problem. Substituting the expression (2.9) for the pressure perturbation and similar expressions for the other flow quantities into the inviscid compressible equations yields the ordinary differential equations for the perturbation amplitudes (Lees and Lin, 1946; Dunn and Lin, 1955). It is straightforward to derive a single equation governing Π, given by

$$\Pi'' - \frac{2U'}{U-c}\Pi' - T[(\alpha^2+\beta^2)T - \alpha^2 M^2 (U-c)^2]\Pi = 0. \tag{2.10}$$

Here, c is the complex phase speed

$$c = \frac{\omega}{\alpha}, \tag{2.11}$$

and primes indicate differentiation with respect to the similarity variable η. In (2.11), α is complex. The real part of α is the wave number in the x direction, while the imaginary part of α indicates whether the disturbance is amplified, neutral, or damped depending on whether α_i is negative, zero, or positive.

It is convenient to transform equation (2.10) to a form analogous to that for two dimensional disturbances. To this end let (Squire, 1933)

$$\hat{\alpha}^2 = \alpha^2 + \beta^2. \tag{2.12}$$

Thus,

$$\alpha = \hat{\alpha}\, cos(\theta), \qquad \beta = \hat{\alpha}\, sin(\theta), \tag{2.13}$$

with θ the angle of propogation of the disturbance wave with respect to the flow direction. Further, define $\hat{M}$ and $\hat{\Pi}$ by

$$\hat{\alpha}\hat{M} = \alpha M, \qquad \hat{\alpha}\hat{\Pi} = \alpha \Pi. \tag{2.14}$$

Applying this transformation to equation (2.10) yields

$$\hat{\Pi}'' - \frac{2U'}{U-c}\hat{\Pi}' - \hat{\alpha}^2 T\,[T - \hat{M}^2(U-c)^2]\hat{\Pi} = 0. \tag{2.15}$$

From the transformation we have

$$\hat{M} = M\,cos(\theta), \tag{2.16}$$

$$c = \frac{\omega}{\alpha} = \frac{\omega}{\hat{\alpha}\,cos(\theta)}. \tag{2.17}$$

Note that T is only a function of M and U, and does not change with the angle of propagation.

The boundary conditions for $\hat{\Pi}$ are obtained by considering the limiting form of equation (2.15) as $\eta \to \pm\infty$. The solutions to (2.15) are of the form

$$\hat{\Pi} \to exp(\pm\,\Omega_{\pm}\,\eta), \tag{2.18}$$

where

$$\Omega^2_{+} = \hat{\alpha}^2[1 - \hat{M}^2(1-c)^2], \qquad \Omega^2_{-} = \hat{\alpha}^2\beta_T\,[\beta_T - \hat{M}^2 c^2]. \tag{2.19}$$

Let us define $c_{\pm}$ to be the values of the phase speed for which $\Omega^2_{\pm}$ vanishes. Thus,

$$c_{+} = 1 - \frac{1}{\hat{M}}, \qquad c_{-} = \frac{\sqrt{\beta_T}}{\hat{M}}. \tag{2.20}$$

Note that c_{+} is the phase speed of a sonic disturbance in the moving stream and c_{-} is the phase speed of a sonic disturbance in the stationary stream. At

$$M = M_{*} \equiv \frac{1 + \sqrt{\beta_T}}{cos(\theta)} \tag{2.21}$$

$c_{\pm}$ are equal.

The nature of the disturbances and the appropriate boundary conditions can now be illustrated by reference to Figure 1, where we plot $c_{\pm}$ versus $\hat{M}$. In what follows we assume that $\hat{\alpha}^2_r > \hat{\alpha}^2_i$. These curves divide the $c_r - \hat{M}$ plane into four regions. If a disturbance exists with a $\hat{M}$ and c_r in region 1, then Ω^2_{+} and Ω^2_{-} are both positive, and the disturbance is subsonic at both boundaries. In region 3, both Ω^2_{+} and Ω^2_{-} are negative and hence the disturbance is supersonic at both boundaries. In region 2, Ω^2_{+} is positive and Ω^2_{-} is negative, and the disturbance is subsonic at $+\infty$ and supersonic at $-\infty$. Finally, in region 4, Ω^2_{+} is negative and Ω^2_{-} is positive so the disturbance is supersonic at $+\infty$ and subsonic at $-\infty$.

If the disturbance wave is subsonic at both $\pm\infty$ (region 1), one can choose the appropiate sign for $\Omega_\pm$ and have decaying solutions. We therefore have an eigenvalue problem. If the disturbance is supersonic at either, or both, boundaries then the asymptotic solutions are purely oscillatory. These solutions are of two types. It is clear that the oscillatory solutions are either incoming or outgoing waves. If one assumes that only *outgoing* waves are permitted, the problem of finding solutions in regions 2, 3, or 4 is again an eigenvalue problem wherein one chooses, as boundary condition, the solutions to (2.15) which yields outgoing waves in the far field.

However if one permits *both* incoming and outgoing waves in the far field it is obvious that there are always solutions for any c in regions 2, 3, and 4. For a given ω, one can always find a continuum of α such that there is a solution to (2.15) with constant amplitude oscillations at either or both boundaries. It is not clear what the physical significance of these solutions is. They appear to be analogous for the infinite domain to the neutral acoustic modes of a waveguide. It might be advantageous to study the dynamics of a wave packet composed of these modes rather than an individual mode. In any event, we will ignore these continuum modes in the remainder of this paper.

One can now see that the appropiate boundary condition for either damped or outgoing waves in the moving and stationary streams are, respectively,

$$\hat{\Pi} \to e^{-\Omega_+ \eta}, \quad \text{if } c > c_+, \qquad \hat{\Pi} \to e^{-i\eta\sqrt{-\Omega^2_+}}, \quad \text{if } c < c_+, \tag{2.22a}$$

$$\hat{\Pi} \to e^{\Omega_- \eta}, \quad \text{if } c < c_-, \qquad \hat{\Pi} \to e^{-i\eta\sqrt{-\Omega^2_-}}, \quad \text{if } c > c_-. \tag{2.22b}$$

To solve the disturbance equation (2.15), we first transform it to a Riccati equation by setting

$$G = \frac{\hat{\Pi}'}{\hat{\alpha} T \hat{\Pi}}. \tag{2.23}$$

Thus, (2.15) becomes

$$G' + \hat{\alpha} T G^2 - \left[\frac{2U'}{U-c} - \frac{T'}{T}\right] G = \hat{\alpha}[T - \hat{M}^2 (U-c)^2]. \tag{2.24}$$

The boundary conditions can be found from (2.22) and (2.23).

The stability problem is thus to solve equation (2.24) for a given real frequency ω, Mach number M, and angle of propagation θ, with U and T defined by (2.5) and (2.8). The eigenvalue is the wavenumber α. Because this equation has a singularity at $U = c$, we shall integrate it along the complex contour (-6,-1) to (6,-1). We iterate on α until the boundary conditions are satisfied.

3. Results. In all of our calculations we have taken $\gamma = 1.4$, $\beta_T = 1/2, 1, 2$, and $0 \le M \le 10$.

For a given real ω the wavenumber, α, must be real for a neutral mode. If $\alpha = 0$, we require that $\hat{\Pi} \to$ *constant* at both boundaries. It can be shown that the corresponding phase speed is $c_\pm$, defined by (2.20), and that there are eigensolutions to (2.24) with this boundary condition.

Lees and Lin (1946) have proven that if a neutral mode is to exist in region 1, the phase speed will be given by $c_N = U(\eta_c)$, where η_c is found from the regularity condition

$$S(\eta) \equiv \frac{d}{d\eta}(T^{-2}\frac{dU}{d\eta}) = 0. \tag{3.1}$$

The corresponding neutral wave number, α_N, must be determined numerically. The eigenfunction is called a regular neutral mode. This result was obtained for the compressible boundary layer but it is easy to extend it to a mixing layer. This criterion has been used by Lessen, et al (1965) and Gropengiesser (1969) to find the phase speed of the regular neutral modes. Note that (3.1) differs from that given by Lees and Lin, Lessen, et al, and Gropengiesser by a factor of T^{-1} because they wrote (3.1) in terms of y and we have chosen to write it in terms of η.

The function $S(\eta)$ is a cubic when U and T are given by (2.5) and (2.8). Explicitely, one finds

$$Z^3 - aZ + b = 0, \tag{3.2}$$

with

$$a = 1 - \frac{4(1+\beta_T)}{(\gamma-1)M^2}, \qquad b = \frac{4(1-\beta_T)}{(\gamma-1)M^2}, \tag{3.3}$$

where

$$Z \equiv tanh(\eta). \tag{3.4}$$

Thus, if Z is a root of (3.2), the phase speed of a *possible* regular neutral mode is

$$c_r = \frac{1}{2}(1+Z). \tag{3.5}$$

Equation (3.2) has either one or three real roots with at least two of the three real roots equal if the discriminant is zero. If we define M_o by

$$M_o = 2(\gamma-1)^{-1/2}\{1 + \beta_T + \frac{3}{2}(1-\beta_T)^{2/3}[(1+\beta_T^{1/2})^{2/3} + (1-\beta_T^{1/2})^{2/3}]\}^{1/2}, \tag{3.6}$$

then there is one real root for $M < M_o$ and three real roots for $M \geq M_o$. In particular, as $M \rightarrow 0$, only one real root exists and is given by

$$Z = \frac{(\beta_T - 1)}{(\beta_T + 1)}, \tag{3.7}$$

with corresponding phase speed

$$c_r = \frac{\beta_T}{(1 + \beta_T)}. \tag{3.8}$$

Also, as $M \to \infty$, there are now three roots $Z = -1, 0, 1$, giving $c_r = 0, 1/2, 1$, respectively.

Recall that the phase speed of a *possible* neutral mode is given by (3.5) for each real root. The theorem of Lees and Lin ensures that this is in fact a regular neutral mode if the wave speed of the mode lies in region 1. If a root of (3.2) yields a phase speed which lies in regions 2, 3, or 4, it may, or may not, be a true regular neutral mode propagating away from the mixing layer. One must determine whether or not, for this phase speed, there is an outgoing solution of (2.24) which satisfies the appropiate boundary conditions.

We, of course, solve for the roots of equation (3.2) directly but insight can be gained by plotting $S(\eta)$ over a range of values of η for various values of M and fixed β_T. Figure 2 is a plot of $S(\eta)$ versus η for $\beta_T = 0.5$ and M = 0, 2, 4, 5.5, 8, 10. One sees that, for $M < M_o = 5.715$, the single real root of (3.2) gives a $c_r < 1/2$; that is the "critical point" is at some $\eta < 0$. However, if $M > M_o$, there are three real roots with one at $\eta < 0$ and the other two at $\eta > 0$.

Gropengiesser, using the Lock profile, stated that if $\beta_T < 0.6$ and $M > 3$, $S(\eta)$ had three zeros. On closer examination, the results shown in his Figure 7 suggests that there will always be three zeros for high enough Mach numbers. He was able to find a neutral solution which satisfied the boundary conditions for only one of these three values and hence ignored the other two zeros of S. It must be noted that Gropengiesser only considered two dimensional disturbances in reaching this conclusion.

Figures 3, 4, and 5 are plots of the wave speed c_r from (3.5), as a function of the Mach number and for $\beta_T = 1/2, 1, 2$, respectively. These figures show that the real zeros of S yield a monotonic curve and a "bubble". It is easy to show that this surface has a saddle point at $\beta_T = 1$ and $M = \sqrt{8/(\gamma-1)}$. The sonic curves $c_\pm$ are also plotted for three dimensional waves with propagation angles of 0^o, 45^o, 60^o, 75^o.

We have carried out numerical calculations in order to determine whether or not the zeros of S always yield the phase speed of a neutral mode. We find, in agreement with Gropengiesser, Lessen, et al, and Lees and Lin, that such is the case only if the solution is subsonic at both boundaries, i.e., it lies in region 1. Gropengiesser concluded that only one of the zeros of S gave the phase speed of a true neutral mode. This is true only if the mode is two-dimensional. One can see from Figures 3-5 that, for any β_T, if the mode is two dimensional ($\theta = 0^o$) there is only one zero of S in region 1. We find that there is a neutral mode corresponding to this value of c_r. For the other zeros of S, we find that there are no solutions which yield damped or outgoing waves if $\theta = 0^o$. However, the sonic speeds $c_\pm$ are functions of the angle of propagation. As θ increases the sonic curves shift towards higher Mach number. Thus for any value of β_T, there will always be some angle of propagation for which all three zeros of S lie in region 1. For example, in Figure 4, if $\theta > 63.44^o$, all three zeros of S correspond to modes which are subsonic at both boundaries. Hence, by the theorem of Lees and Lin, there are now three neutral modes with phase speeds equal to the value of U at the corresponding values of η_c. Thus, the significance of the three real zeros of S only becomes apparent at very large angles of propagation.

There can also be singular neutral modes; those which do not satisfy (3.1) but are solutions of (2.24) with only outgoing or damped waves at $\pm\infty$. It is obvious that these are singular

eigenfunctions. The singularity will be removed by the action of non-zero viscosity. Hence we can regard these singular modes as the limit of some viscous, spatial stability modes as the Reynolds number approaches infinity.

One can find these modes by obtaining numerical solutions of (2.24) which are either decaying (if the disturbance is subsonic) or outwardly propagating (if the disturbance is supersonic) at $\pm \infty$, without requiring that (3.1) be satisfied. We have carried out such calculations and found that, for any value of β_T, there is always one singular neutral mode in region 2 of the $c_r - M$ plane and another singular neutral mode in region 4.

Results for the two dimensional neutral modes are shown in Figures 6, 7, and 8. Figures 6a, 7a, and 8a are plots of the phase speed as a function of the Mach number and for $\beta_T = 1/2$, 1, 2, respectively. The dashed curves are the neutral sonic modes with phase speeds $c_\pm$ and $\alpha = 0$. For each value of β_T there is a single neutral wave in region 1. As M is increased, this mode crosses over the sonic curve into either region 2 or 4 and is transformed into a singular neutral mode. If $\beta_T > 1$, this mode becomes a fast mode whose phase speed approaches one as M goes to infinity. If $\beta_T < 1$, the mode becomes a slow mode whose phase speed approaches zero as the Mach number increases. In each case, there is also another singular neutral mode, fast if $\beta_T < 1$ and slow if $\beta_T > 1$. These appear at Mach numbers slighly smaller than M_*. If $\beta_T = 1$, the subsonic mode splits symmetrically into a fast and a slow mode. Note that for a small range of M around M_* there can be more than three different neutral modes in addition to the two sonic modes.

The corresponding wave numbers, displayed in Figures 6b-8b, decrease as the Mach number increases from 0 to M_*. The mode with the larger wave number is always the regular mode and its singular continuation at higher Mach numbers. The other mode always has a smaller wave number and hence a longer wave length. The discontinuity in the slope of the wave number curves is due to the transformation from a regular to a singular mode when crossing a sonic curve. For $\beta_T = 1$, both modes have the same value of the wave number at any $M > M_*$. For all β_T, the wave numbers increase slightly with Mach number.

Finally, the corresponding frequencies, displayed in Figures 6c-8c, decrease as the Mach number increases from 0 to M_*. For $M > M_*$, the frequency of one of the singular modes increases and that of the other decreases. This, combined with the relatively constant values of the wave numbers, leads to the appearence of fast and slow modes. If $\beta_T < 1$, the curves of ω_N for the singular modes must cross at some $M > M_*$. Thus, one will have two different neutral modes at the same frequency and Mach number but with different wave numbers. If $\beta_T > 1$ the neutral modes have quite different frequencies.

Based on our numerical results, we find that for M = 0,

$$c_N = \frac{\beta_T}{(1+\beta_T)}, \qquad \alpha_N = \frac{1+\beta_T}{2\beta_T}\cos(\theta), \qquad \omega_N = \frac{\cos(\theta)}{2}, \tag{3.9}$$

consistent with (3.8) and Figures 6-8.

Figures 9 thru 13 are plots of selected neutral eigenfunctions for $\beta_T = 1$. These plots show the variation of Π with η_r on the contour $\eta_i = -1$. All of these have been normalized so that the

maximum of the absolute value of Π is unity. The eigenfunction shown in Figure 9 is a regular neutral mode at $M = 1$. The wave is subsonic at both boundaries, so Π decays exponentially away from the mixing layer. Note the rapid variation of the phase near $\eta_r = 0$. Figures 10 and 11 are plots of the two singular neutral modes of Π at $M = 2.5$. The eigenvalue for the eigenfunction in Figure 10 lies in region 2 so the mode is subsonic at $+\infty$ and supersonic at $-\infty$. The eigenvalue for the mode shown in Figure 11 lies in region 4 and has just the opposite behavior. Both modes show exponential decay in the subsonic region and oscillations with constant amplitude and phase in the supersonic region. Both show a rapid phase shift near the center of the mixing layer. Finally, Fiqures 12 and 13 are plots of the singular neutral eigenfunctions at $M = 5$. As before, the eigenvalue of Figure 12 lies in region 2 and that of Figure 13 in region 4. The behavior of these eigenfunctions is quite similar to that of the modes at $M = 2.5$, but note that the wave length of the oscillation decreases as the Mach number increases.

As was stated above all three real roots of S can be the phase speeds of regular neutral modes if the disturbance wave is three dimensional. As an example, we show in Figure 14 results for the neutral modes at $\beta_T = 1$ and $\theta = 75°$. From M = 0 up to $M_o = 4.472$ there is a single regular neutral mode with $c_N = 0.5$ and both α_N and ω_N monotonically decreasing. For $M \geq M_o$, S has three real roots and these are the phase speeds of three regular neutral modes for $M_o \leq M \leq 5.15$. One of these modes has $c_N = 0.5$, another has an increasing c_N and the other a decreasing c_N. From 14b and 14c one can see that α_N and ω_N for the mode $c_N = 0.5$ decrease monotocially until they vanish at $M_* = 7.727$. The wave numbers of the other two neutral waves increase with M beyond M_o. The curves of α_N for these modes show a discontinuity in slope at $M = 5.15$ as they intersect the sonic curves and are transformed into singular neutral modes. The phase speeds of these singular modes are only slightly different from, and appear to be asymptotic to, the values obtained from the zeros of S. Finally, the curves of ω_N split at M_o with that of the fast mode increasing and that of the slow mode decreasing. These curves also show discontinuities in slope at $M = 5.15$.

As would be expected there exists a band of unstable waves adjacent to the neutral modes. In particular, for Mach numbers greater than M_* the bands of unstable modes lies between the singular neutral curve and the sonic curve (see Figures 6a-8a). We have carried out calculations to determine the growth rates of these unstable modes. Some of these results are shown in Figures 15, 16, and 17 where we have plotted the maximum growth rate $(-\alpha_{i_{max}})$ for two dimensional modes as a function of Mach number and for $\beta_T = 1/2, 1, 2$, respectively. Each of these figures shows two curves. The curve giving the larger values of the growth rate is that of the first group of unstable waves; that group which exists for $M < M_*$. The second curve gives the maximum growth rate for the group of unstable waves which appears at Mach numbers slightly below M_*.

We find, in agreement with Gropengiesser, that the flow becomes less unstable as the stationary gas becomes hotter. Gropengiesser also stated that the growth rates decrease with increasing Mach number over the range of Mach numbers which he studied. This is certainly true for $M < M_*$, where one can see there is a very rapid decrease in the maximum growth rate with increase in Mach number. For Mach numbers greater than M_*, the rate of decrease is much smaller and eventually, at some moderate value of M, the growth rate begins to increase. Note that at higher Mach number the growth rate increases with a decrease of β_T. Gropengiesser did not see

this because he only carried out calculations up to M = 3.

Gropengiesser said that he found a second unstable mode for two dimensional waves in a narrow range of Mach numbers, $1.54 < M < 1.73$. He also stated that this second mode had a growth rate comparable to the first when $\theta = 30^o$ and $\beta_T = 0.6$. Finally, he indicated that the growth rate of the second mode decreased sharply as β_T was increased. It is clear from the results presented in Figures 6, 7, 8, and 14 that there will *always* be two groups of unstable modes if $M \geq M_*$. Of course these groups may have different ranges of frequencies and will have quite different phase speeds. The varation of the maximum growth rate of the second group of unstable two dimensional waves is given by the second curves in Figures 15, 16, and 17. For all values of β_T the growth rate for the second group increases over a small range of M, and than decreases. At a moderate value of M the growth rate begins to increase slowly with M. This is more readily apparent for $\beta_T = 2$ than for the other values. The maximum growth rates for the second group are generally rather small, but are comparable to those of the first group for larger values of β_T.

In order to display the characteristics of both of these unstable waves in more detail we consider a single case, that of $\beta_T = 2$. The phase speed, wave numbers, and frequencies are shown in Figure 8 and the maximum growth rates in Figure 17. The second group of unstable waves only exist for $M > M_* = 2.414$. From Figure 8 one can see that the first group is the fast waves and the second group the slow waves. Figure 18 is a plot of the growth rate, $-\alpha_i$, of the unstable two dimensional waves at M = 2.5. This value of M was chosen so as to be slightly above M_*. The upper curve is that of the first group, the fast modes. There are two neutral frequencies, $\omega_N = 0$ corresponding to the sonic mode c_+ and the other, $\omega_N = 0.24$ corresponds to that of the fast singular neutral mode. From Figure 8 one can see that the phase speeds of these modes lie in the range 0.58 to 0.73, suggesting that the wave packets of these modes would have relatively little dispersion. The upper curve has two maxima, one at $\omega = 0.025$ and the other at $\omega = 0.09$. These are nearly the same size, but that of the larger value of ω is much broader.

The growth rates for the second group of waves are shown by the lower curve in Figure 18. These are the slow modes, see Figure 8, with phase speeds between 0.5 and 0.58. It is clear that at this Mach number the phase speed of the fast and slow modes are not much different, but the slowest of the first group is faster than the fastest of the second group. The second group of unstable modes has a maximum growth rate of about two-thirds of that of the first group. However, the band of unstable frequencies is much narrower for the second group than for the first. The zero of the growth rate at $\omega_N = 0$ corresponds to the sonic curve c_- and the other zero to the slow singular neutral mode.

The results shown in Figure 19 are similar to that of Figure 18 but for M = 5. The maximum growth rates of both groups of waves at M = 5 are only about one-fifth of those of M = 2.5, but the relative sizes of each group are about the same. The fast modes exist over a frequency range about the same as at M = 2.5, but the phase speeds all lie in the range of 0.8 to 0.87. The frequency band of the slow modes is much less at M = 5 than at 2.5. The phase speeds of the waves in the second group are much different from those in the fast group at this Mach number, ranging from 0.25 to 0.28. Thus, at high Mach numbers the amount of dispersion is reduced.

The results of Figure 18 and 19 are for two dimensional waves. The same general behavior is also characteristic of three dimensional modes. Figure 20a shows the growth rate of the fast modes and 20b the growth rates of the slow modes as a function of frequency for different angles of propagation at $\beta_T = 2$ and $M = 2.5$. The maximum growth rate of the fast modes increases as θ increases up to about 60^o and then decreases for larger angles of propagation. The range of unstable frequencies decreases as θ increases. The results given in 20b show that the slow mode has a different behavior. The maximum growth rate occurs for two dimensional waves and decreases as the angle increases and essentially disappears for $\theta > 20^o$, because then the mode becomes subsonic.

Figure 21 shows the variation of the growth rate with frequency for both fast and slow modes for various angles of propagation at $\beta_T = 2$ and $M = 5$. The results are similar to those of Figure 20. As the angle of propagation increases the fast modes experience a decrease in the range of unstable frequencies and an increase in the growth rate; the maximum occurs at about $\theta = 75^o$. The slow modes do not show much of an increase in maximum growth rate with angle of propagation.

In addition to the two groups of unstable waves discussed above, we have found another group of two and three dimensional unstable waves which have very large growth rates and very small phase speeds. These modes were found for $\beta_T = 1/2, 1, 2$ at $M = 5$. We will present results here only for $\beta_T = 1$. Figure 22 shows the variation of the growth rate of these modes with frequency for a number of propagation angles from 0^o to 75^o. The growth rates are very large, about 1.8 for $\theta = 0^o$ at $\omega = 0$. The growth rates decrease slowly with increasing θ and ω but are still quite large at $\theta = 75^o$ and $\omega = 0.024$. The phase speeds of these modes are shown in Figures 23a and 23b for a number of propagation angles. The results given in these figures show that the phase speeds of these modes is always less than 0.01. As θ is decreased from 75^o to 0^o, the range of permissible frequencies decreases until, at $\theta = 0^o$, we only have a two dimensional standing wave.

Figures 24 are plots of the eigenfunction for these very slow modes as a function of η_r along the contour $\eta_i = -1$ for $\theta = 60^o$. The frequency, wave number, and phase speed of these modes are given in the captions of Figure 24. The eigenfunction shown in 24a is that at the maximum phase speed and the others, 24b and 24c, correspond to the standing waves ($c_r = 0$) at $\omega = 0$ and 0.021226. Apart from the very large growth rates of these modes, the only unusual feature appears to be the double phase shift near $\eta_r = 0$. Similarly, very slow and very unstable modes have also been found for the other values of β_T. We will present a detailed study of these modes at a later date.

4. Summary and Conclusions. In this work we have considered the spatial stability problem for the compressible mixing layer with the mean velocity profile approximated by the hyperbolic tangent. We have found that there is only a single regular neutral mode for two dimensional waves, but that there can be three for three dimensional waves. The regular neutral disturbances are always subsonic at the boundaries. These modes cease to exist at the Mach number at which their phase speed equals that of a sonic wave. Beyond the sonic curves the modes are transformed into singular neutral modes which are subsonic at one boundary and supersonic at the other. We have not found any singular neutral waves which are supersonic at both boundaries.

There are always at least two bands of unstable frequencies for Mach numbers greater than M_*. One of these bands is a group of fast and the other a group of slow unstable waves. These groups of unstable waves lie in the frequency bands between zero, corresponding to the sonic modes, and the frequency of the singular neutral modes. Because these frequency bands always overlap for some range of frequencies, there exist two unstable modes at a fixed M and β_T for every frequency in this range. The phase speeds of both the fast and slow modes have a small range about the average, so that little dispersion of wave packets is expected, with a reduction in the dispersion as the Mach number is increased.

Three dimensional disturbances show the same general characteristics as two dimensional disturbances. There is always a range of propagation angles for which both the fast and slow unstable modes exists. We also find, in agreement with previous studies, that the maximum growth rate for any β_T and M occurs for three dimensional modes.

A decrease in β_T results in an increase in the growth rate of the unstable modes at any Mach number. An increase in the Mach number at a fixed β_T results in a decrease in the growth rate up to a Mach number of three or four. For higher Mach numbers, the growth rate increases slowly. Even at Mach 10, the growth rates are small compared to those of low subsonic speeds. This, combined with the fact that the unstable modes have little dispersion, is the possible mechanism responsible for the observed increase in the flow stability.

We have found a group of very slowly propagating, highly unstable modes at M = 5. These modes are both two and three dimensional and all have large growth rates, of O(1), with the maximum growth rate ocurring for the two dimensional wave at $\omega = 0$. All of these waves have phase speeds which are less than 0.01 and hence are nearly standing waves. We will present a detailed study of these modes at a later date.

If these modes could be excited in a mixing layer, we believe that they would lead to a rapid transition to turbulence because of their large growth rates. Transition would then yield enhanced mixing between the two streams.

REFERENCES

Chapman, D. R. 1950 Laminar mixing of a compressible fluid. NACA Rep. 958.

Dunn, D. W. & Lin, C. C. 1955 On the stability of the laminar boundary in a compressible fluid. J. Aero. Sci. 22, 455-477.

Gropengiesser, H. 1969 On the Stability of Free Shear Layers in Compressible Flows. (in German), Deutsche Luft. und Raumfahrt, FB 69-25, 123 pp. Also, NASA Tech. Translation NASA TT F-12,786.

Ho, C. M. & Huerre, P. 1984 Perturbed free shear layers. Ann. Rev. Fluid Mech. 16, 365-424.

Jackson, T. L. & Hussaini, M. Y. 1988 An Asymptotic Analysis of Supersonic Reacting Mixing Layers. Comb. Sci. Tech. 57, 129-140.

Kumar, A., Bushnell, D. M. & Hussaini, M. Y. 1987 A mixing augmentation technique for hypervelocity scramjets. AIAA Paper No. 87-1882.

Lees, L. & Lin, C. C. 1946 Investigation of the stability of the laminar boundary layer in a compressible fluid. NACA Tech. Note 1115.

Lessen, M., Fox, J. A. & Zien, H. M. 1965 On the Inviscid Stability of the Laminar Mixing of Two Parallel Streams of a Compressible Fluid. J. Fluid Mech. 23, 355-367.

Lessen, M., Fox, J. A. & Zien, H. M. 1966 Stability of the Laminar Mixing of two Parallel Streams with Respect to Supersonic Disturbances. J. Fluid Mech. 25, 737-742.

Lock, R. C. 1951 The velocity distribution in the laminar boundary layer between parallel streams. Quart. J. Mech. and Appl. Math. 4, 42-63.

Mack, L. M. 1984 Boundary layer linear stability theory. In *Special Course on Stability* and *Transition of Laminar Flow*. AGARD Report R-709, 3-1 to 3-81.

Michalke, A. 1972 The instability of free shear layers. Progress in Aerospace Sciences. 12, 213-239.

Monkewitz, P. A. & Huerre, P. 1982 Influence of the Velocity Ratio on the Spatial Instability of Mixing Layers. The Physics of Fluids 25, 1137-1143.

Papamoschou, D. & Roshko, A. 1986 Observations of supersonic free-shear layers. AIAA Paper No. 86-0162.

Stewartson, K. 1964 *The Theory of Laminar Boundary Layers in Compressible Fluids*. Oxford University Press, Great Britain.

Squire, H. B. 1933 On the stability for three dimensional disturbances of viscous fluid flow between parallel walls. Proc. Roy. Soc. A. 143, 621-628.

FIGURE CAPTIONS

Figure 1. Plots of the sonic speeds $c_{\pm}$ versus Mach number.

Figure 2. Plot of $S(\eta)$ for $\beta_T = 0.5$ and for M = 0, 2, 4, 5.5, 8, 10.

Figure 3. Plot of the real roots of S versus Mach number for $\beta_T = 0.5$. Sonic curves are also shown for propagation angles 0^o, 45^o, 60^o, 75^o.

Figure 4. Plot of the real roots of S versus Mach number for $\beta_T = 1$. Sonic curves are also shown for propagation angles 0^o, 45^o, 60^o, 75^o.

Figure 5. Plot of the real roots of S versus Mach number for $\beta_T = 2$. Sonic curves are also shown for propagation angles 0^o, 45^o, 60^o, 75^o.

Figure 6. Plots of two dimensional neutral curves for $\beta_T = 0.5$ versus Mach number: 6a phase and sonic speeds; 6b wave number; 6c frequency.

Figure 7. Plots of two dimensional neutral curves for $\beta_T = 1$ versus Mach number: 7a phase and sonic speeds; 7b wave number; 7c frequency.

Figure 8. Plots of two dimensional neutral curves for $\beta_T = 2$ versus Mach number: 8a phase and sonic speeds; 8b wave number; 8c frequency.

Figure 9. Plot of the two dimensional regular neutral eigenfunction $\Pi(\eta)$. The solid curve corresponds to the real part and the dashed curve to the imaginary part. M = 1, $\beta_T = 1$, $\omega_N = 0.390495$, $\alpha_N = 0.780991$, $c_N = 0.5$.

Figure 10. Plot of the two dimensional singular neutral eigenfunction $\Pi(\eta)$. The solid curve corresponds to the real part and the dashed curve to the imaginary part. M = 2.5, $\beta_T = 1$, $\omega_N = 0.173064$, $\alpha_N = 0.252214$, $c_N = 0.68618$.

Figure 11. Plot of the two dimensional singular neutral eigenfunction $\Pi(\eta)$. The solid curve corresponds to the real part and the dashed curve to the imaginary part. M = 2.5, $\beta_T = 1$, $\omega_N = 0.079151$, $\alpha_N = 0.252214$, $c_N = 0.31382$.

Figure 12. Plot of the two dimensional singular neutral eigenfunction $\Pi(\eta)$. The solid curve corresponds to the real part and the dashed curve to the imaginary part. M = 5, $\beta_T = 1$, $\omega_N = 0.184813$, $\alpha_N = 0.215661$, $c_N = 0.85696$.

Figure 13. Plot of the two dimensional singular neutral eigenfunction $\Pi(\eta)$. The solid curve corresponds to the real part and the dashed curve to the imaginary part. M = 5, $\beta_T = 1$, $\omega_N = 0.030847$, $\alpha_N = 0.215661$, $c_N = 0.14303$.

Figure 14. Plots of three dimensional ($\theta = 75^o$) neutral curves for $\beta_T = 1$ versus Mach number: 14a phase and sonic speeds; 14b wave number; 14c frequency.

Figure 15. Plot of maximum growth rate for two dimensional waves versus Mach number for $\beta_T = 0.5$.

Figure 16. Plot of maximum growth rate for two dimensional waves versus Mach number for $\beta_T = 1$.

Figure 17. Plot of maximum growth rate for two dimensional waves versus Mach number for $\beta_T = 2$.

Figure 18. Plot of growth rates for two dimensional waves versus frequency for $\beta_T = 2$ and M = 2.5.

Figure 19. Plot of growth rates for two dimensional waves versus frequency for $\beta_T = 2$ and M = 5.

Figure 20. Plot of growth rates for three dimensional waves versus frequency for $\beta_T = 2$, $M = 2.5$: 20a first modes, $\theta = 0^o, 20^o, 30^o, 45^o, 60^o, 75^o$; 20b second modes, $\theta = 0^o, 10^o, 15^o, 20^o$.

Figure 21. Plot of growth rates for three dimensional waves versus frequency for $\beta_T = 2$, $M = 5$: 21a first modes, $\theta = 0^o, 30^o, 45^o, 60^o, 75^o$; 21b second modes, $\theta = 0^o, 30^o, 45^o, 60^o$.

Figure 22. Plot of growth rates for two and three dimensional waves versus frequency for $\beta_T = 1$, M = 5, and $\theta = 0^o, 30^o, 45^o, 60^o, 75^o$.

Figure 23. Plot of phase speeds for two and three dimensional waves versus frequency for $\beta_T = 1$, M = 5: 23a $\theta = 60^o, 65^o, 70^o, 75^o$; 23b $\theta = 0^o, 30^o, 45^o$.

Figure 24. Plot of the three dimensional ($\theta = 60^o$) singular eigenfunctions $\Pi(\eta)$. The solid curve corresponds to the real part and the dashed curve to the imaginary part at M = 5 and $\beta_T = 1$: 24a $\omega = 0.015$, $\alpha_r = 0.03864$, $\alpha_i = -0.48525$, $c_r = 0.00245$; 24b $\omega = 0.021226$, $\alpha_r = 0.0$, $\alpha_i = -0.41899$, $c_r = 0.0$; 24c $\omega = 0.0$, $\alpha_r = 0.0$, $\alpha_i = -0.66974$, $c_r = 0.0$.

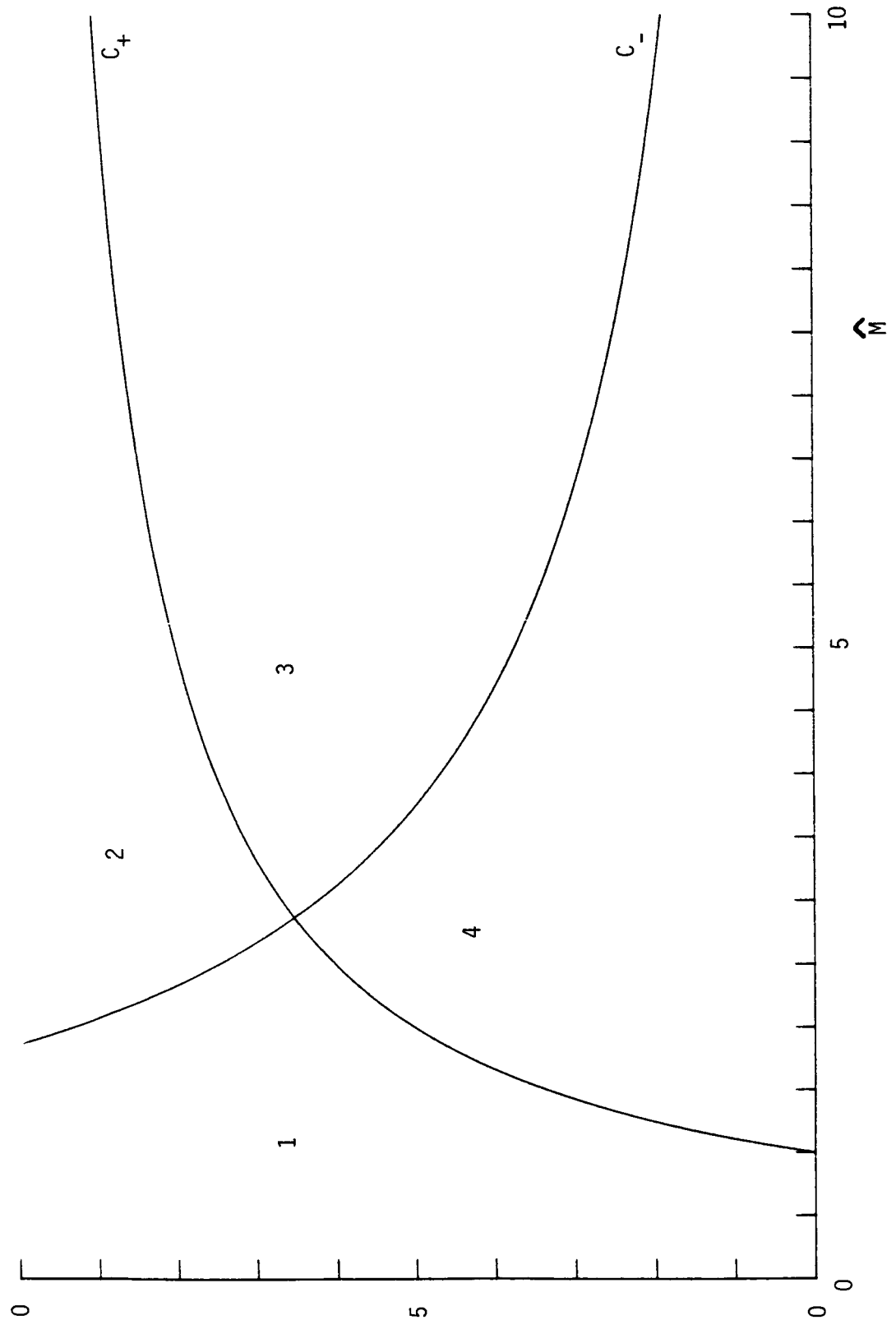

Figure 1.

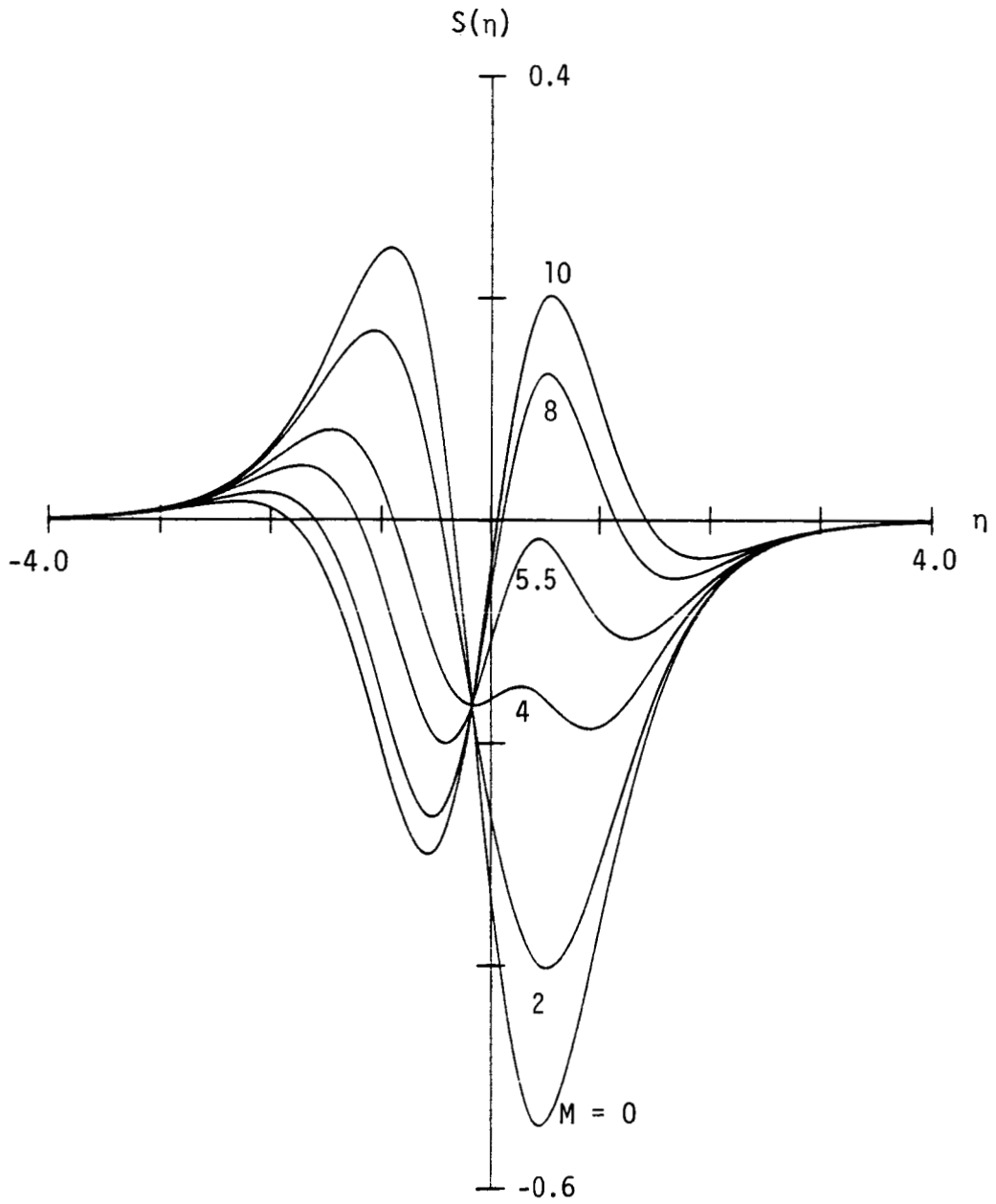

Figure 2.

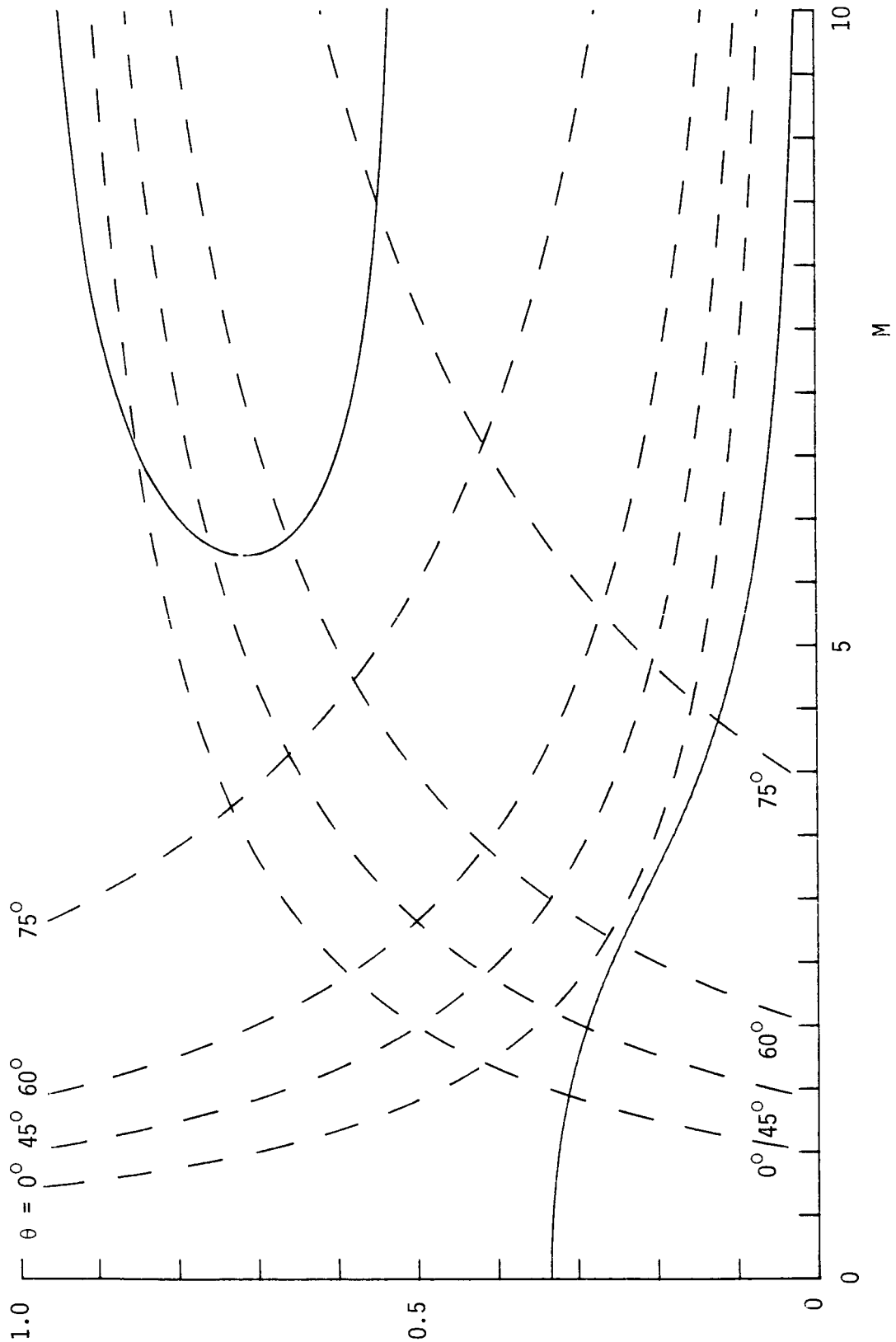

Figure 3.

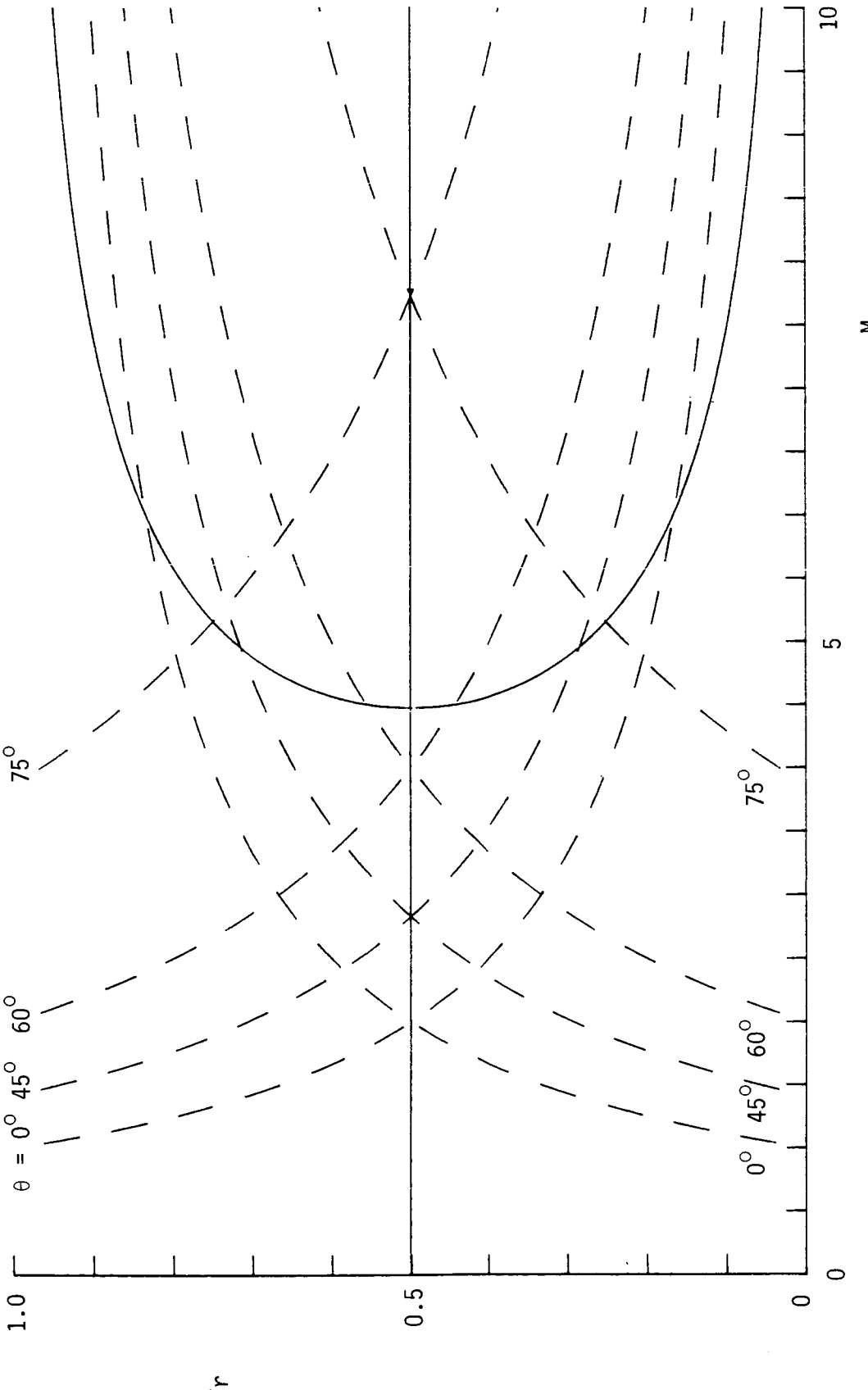

Figure 4.

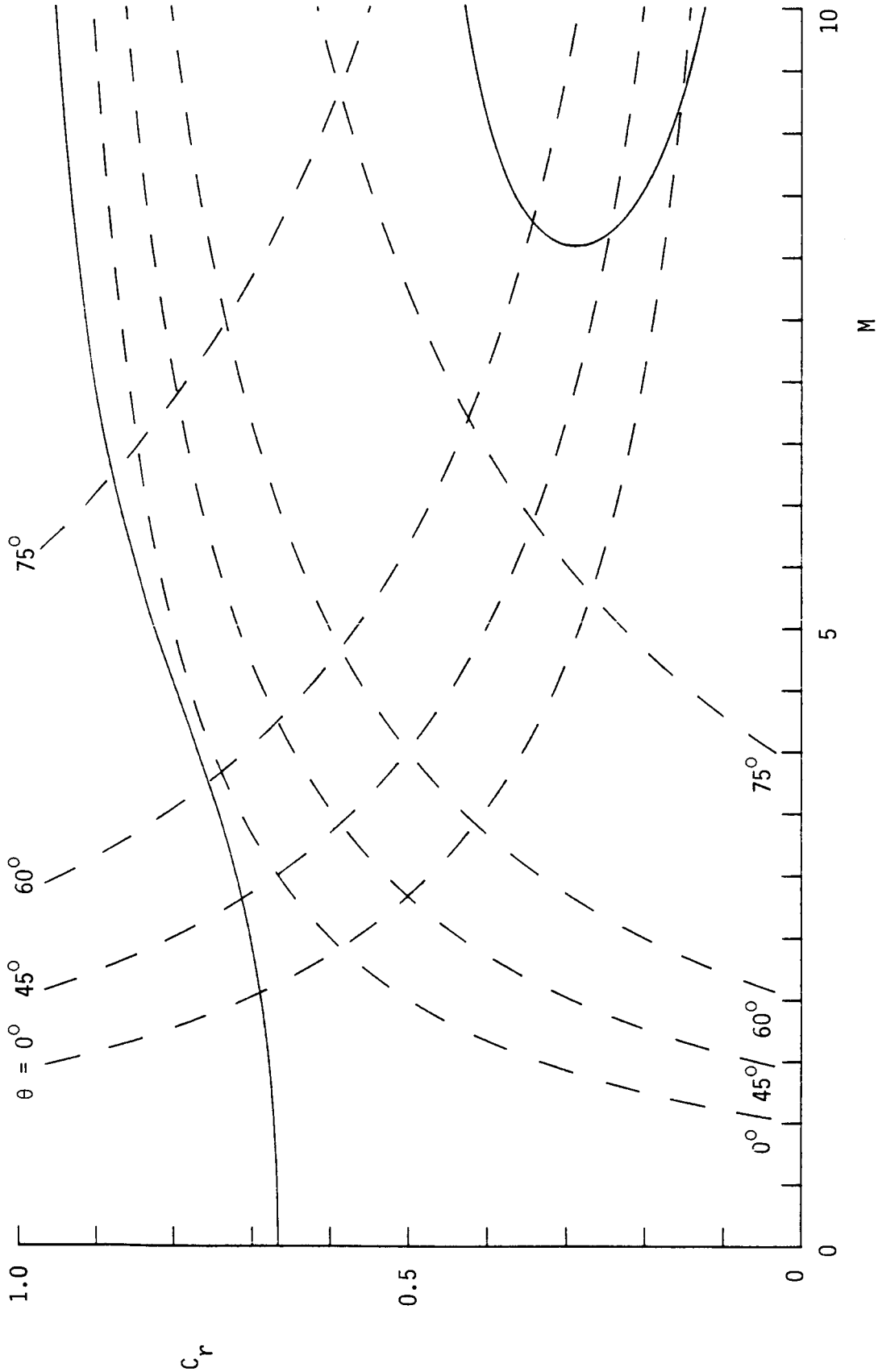
1.0
0.5
0
C_r
0
5
10
M
$\theta = 0^\circ$
45°
60°
75°
0°
45°
60°
75°

Figure 5.

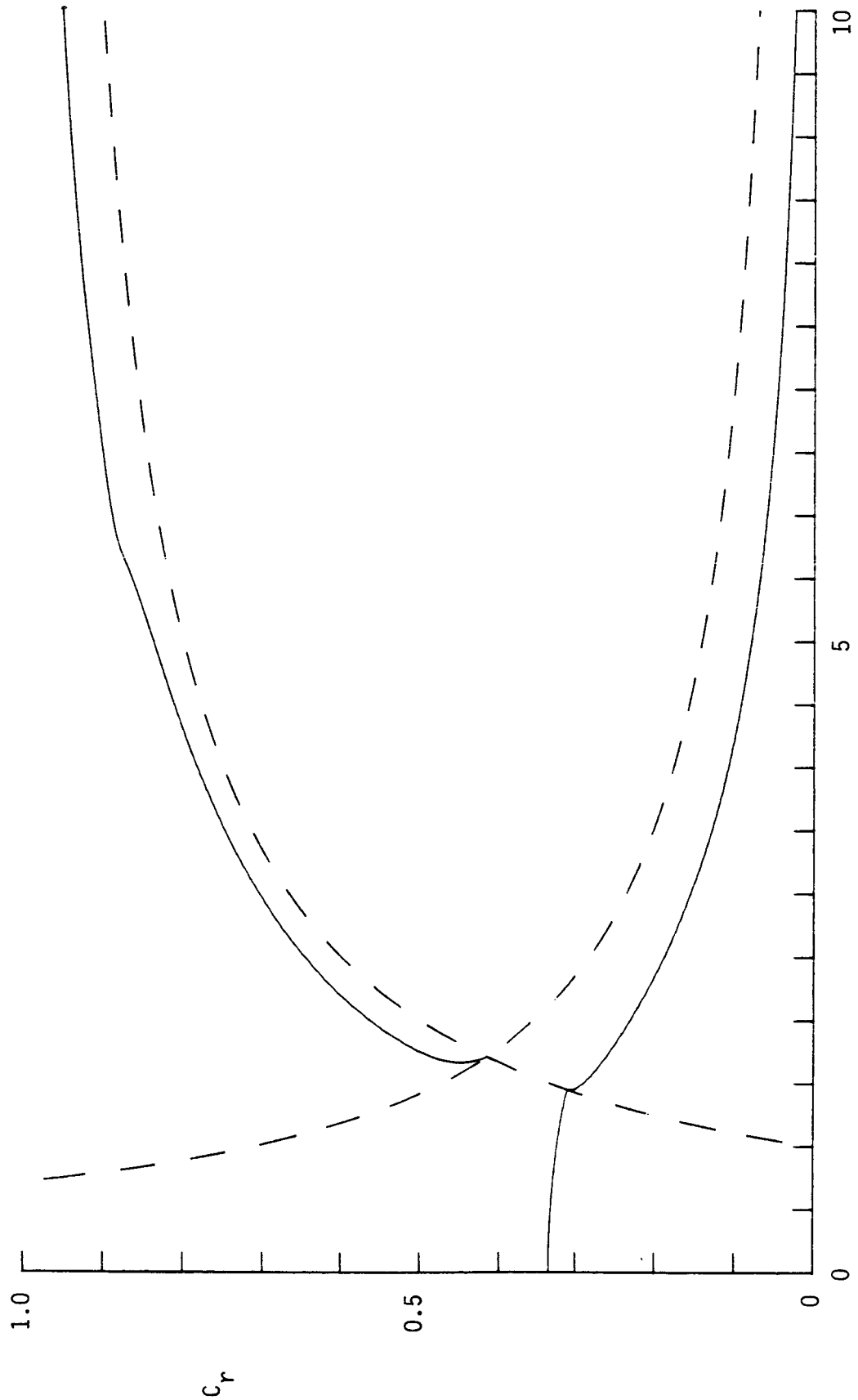

Figure 6a.

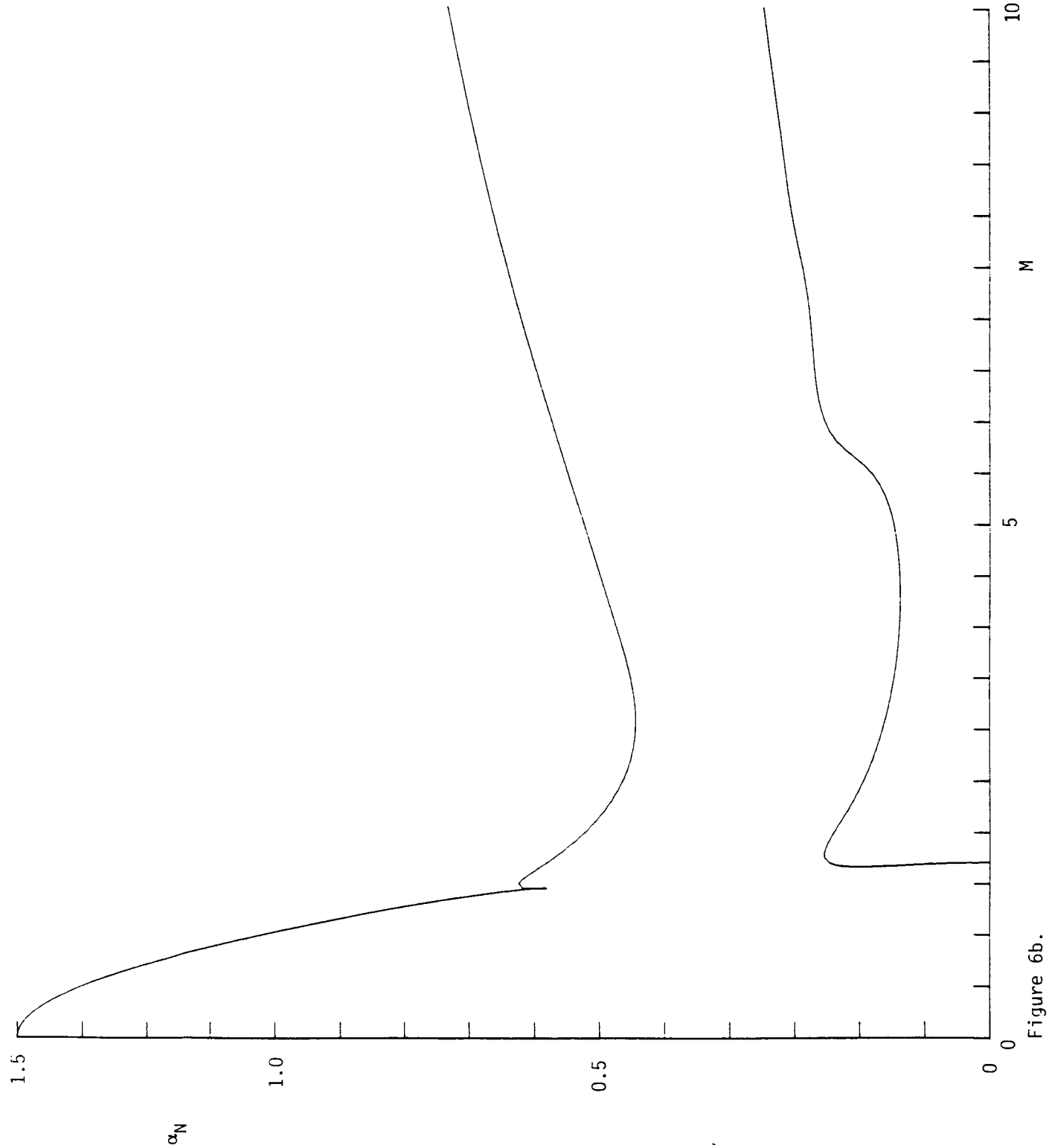

Figure 6b.

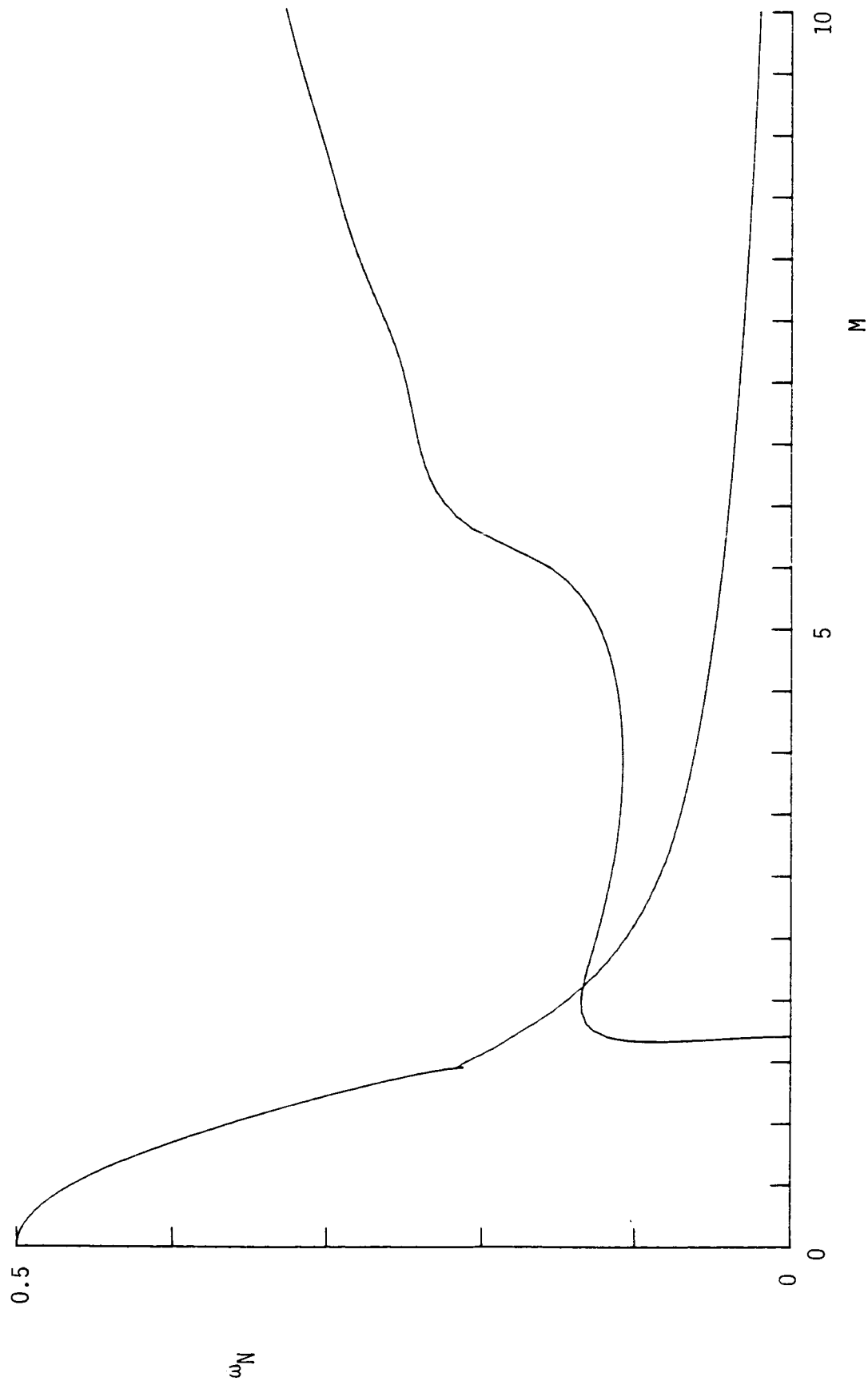

Figure 6c.

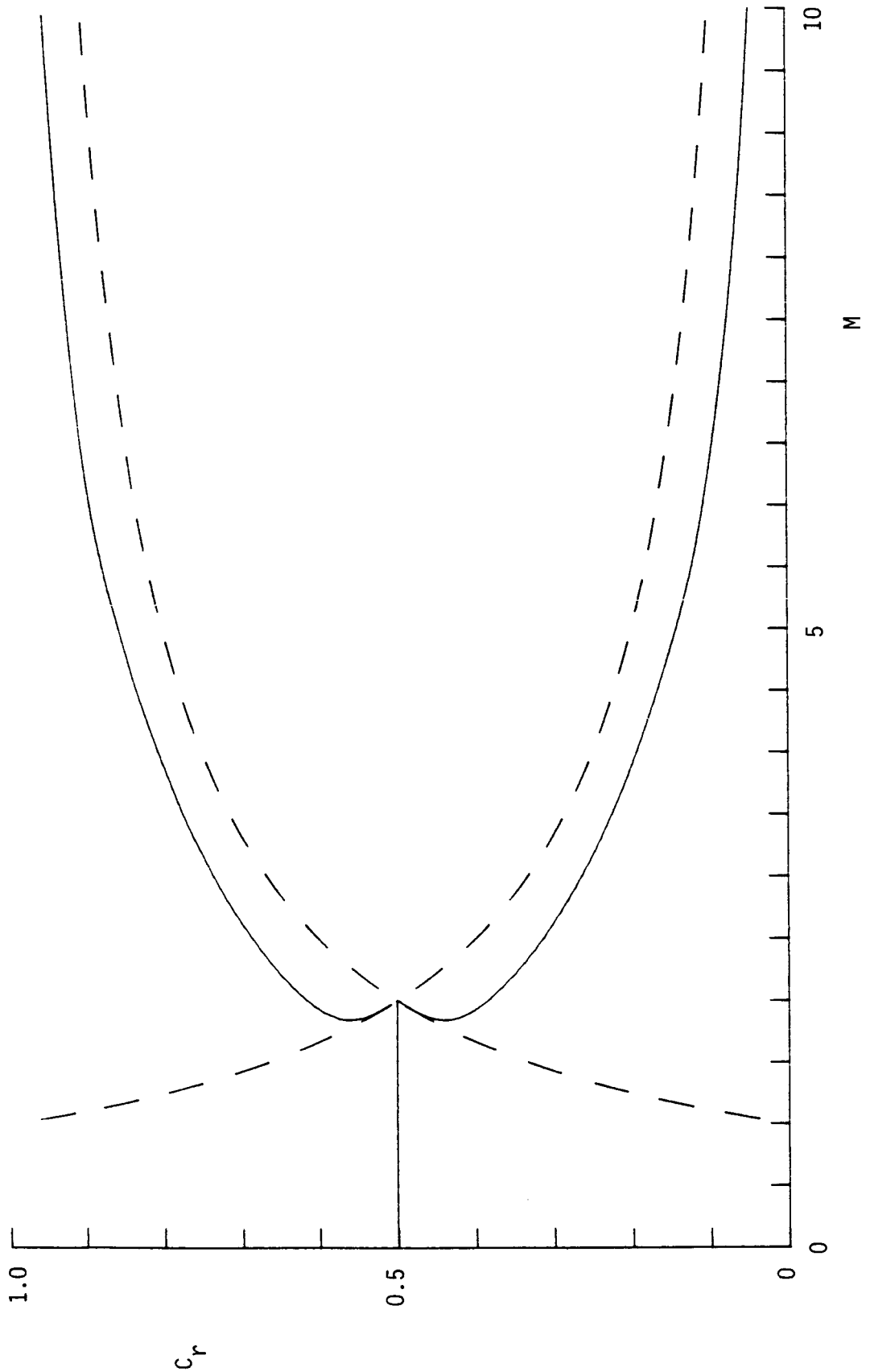

Figure 7a.

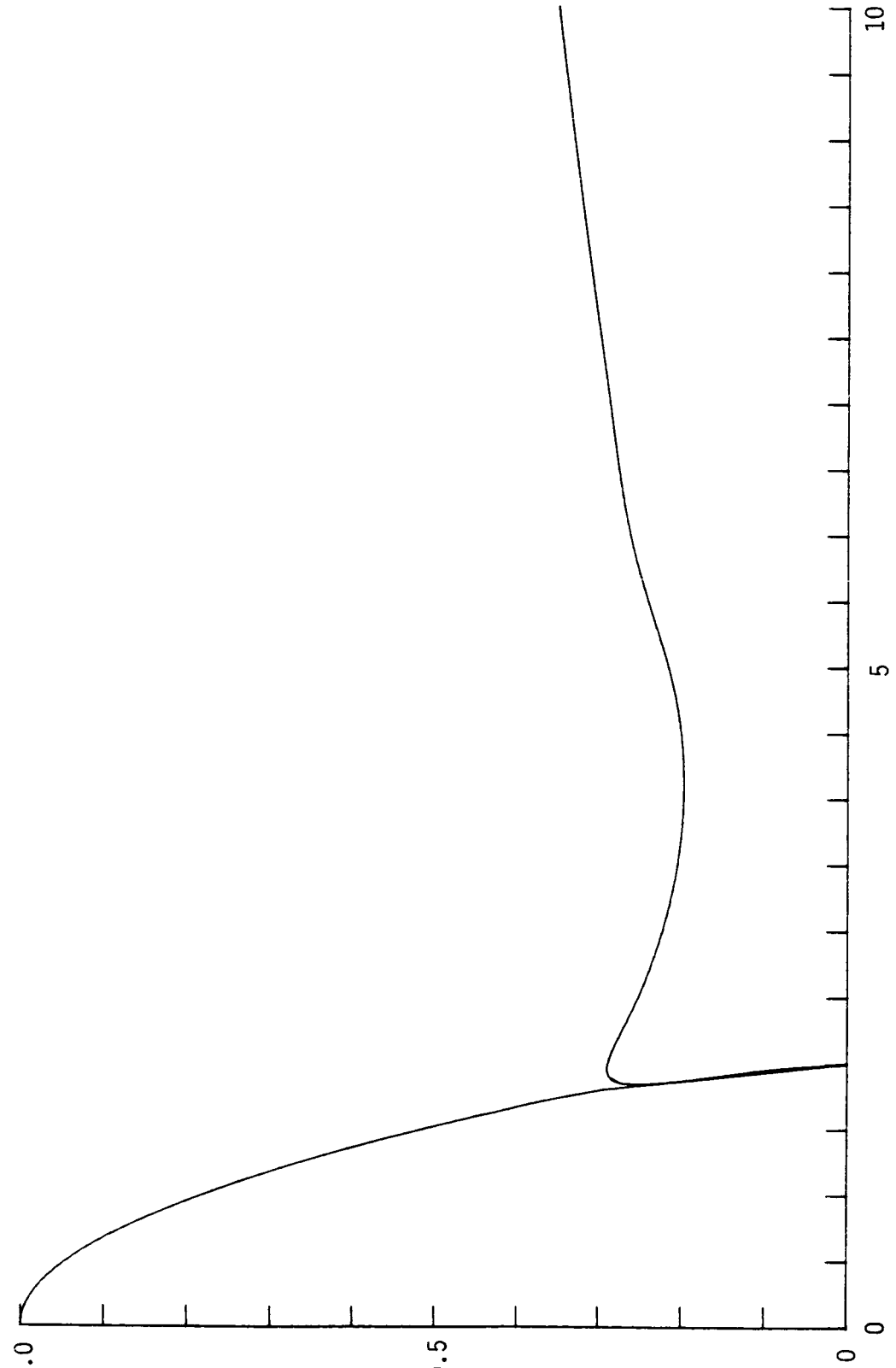

Figure 7b.

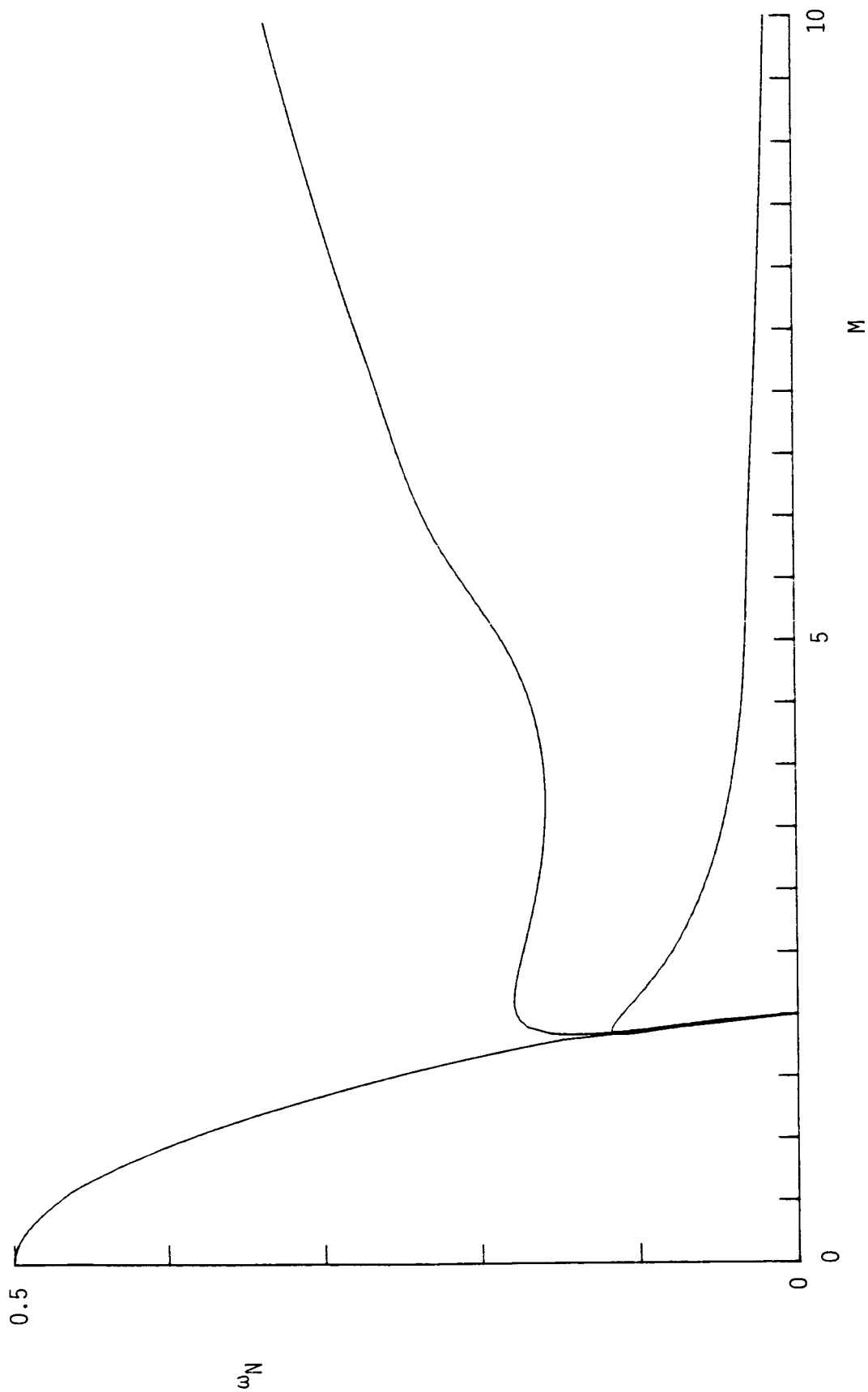

Figure 7c.

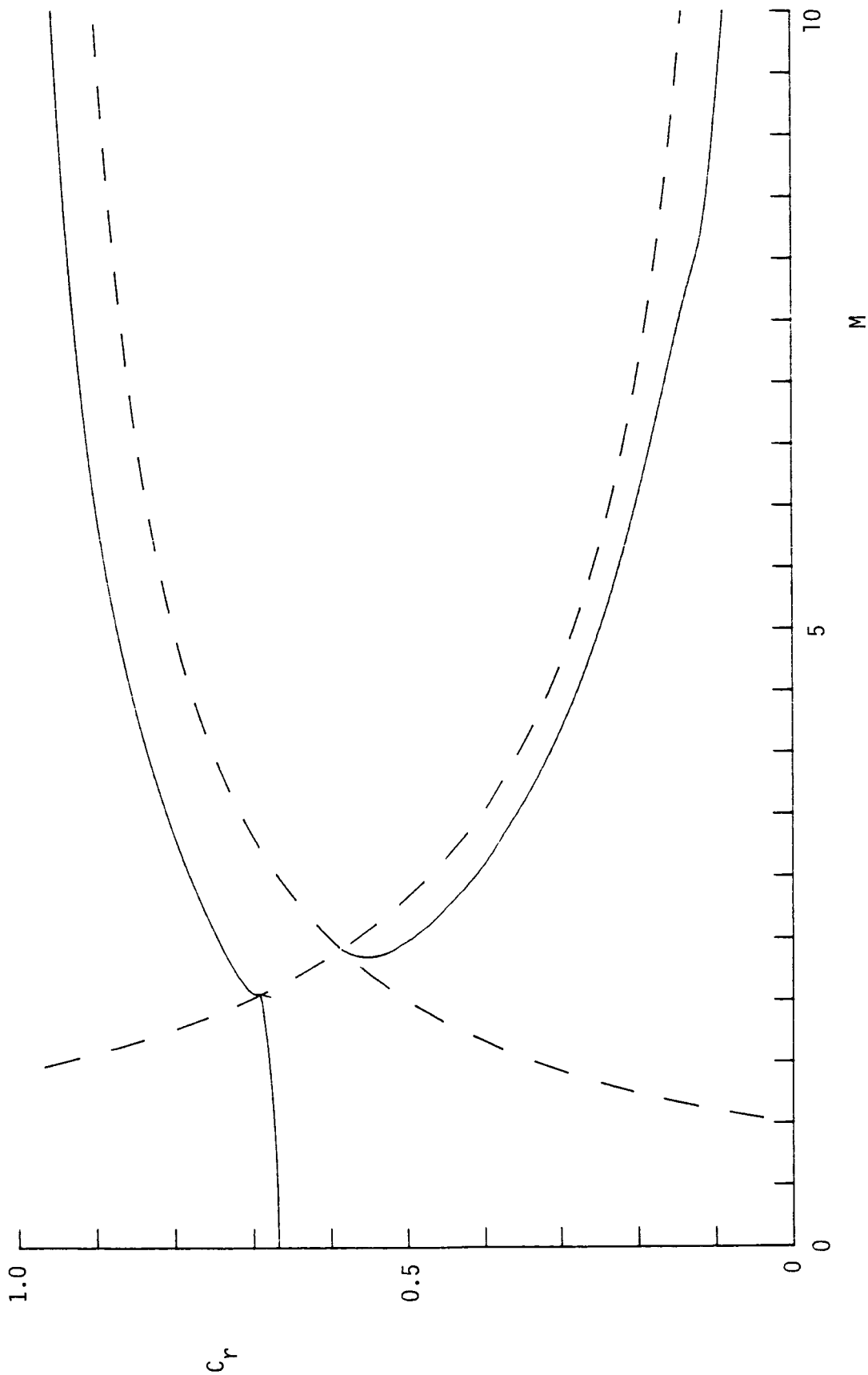

Figure 8a.

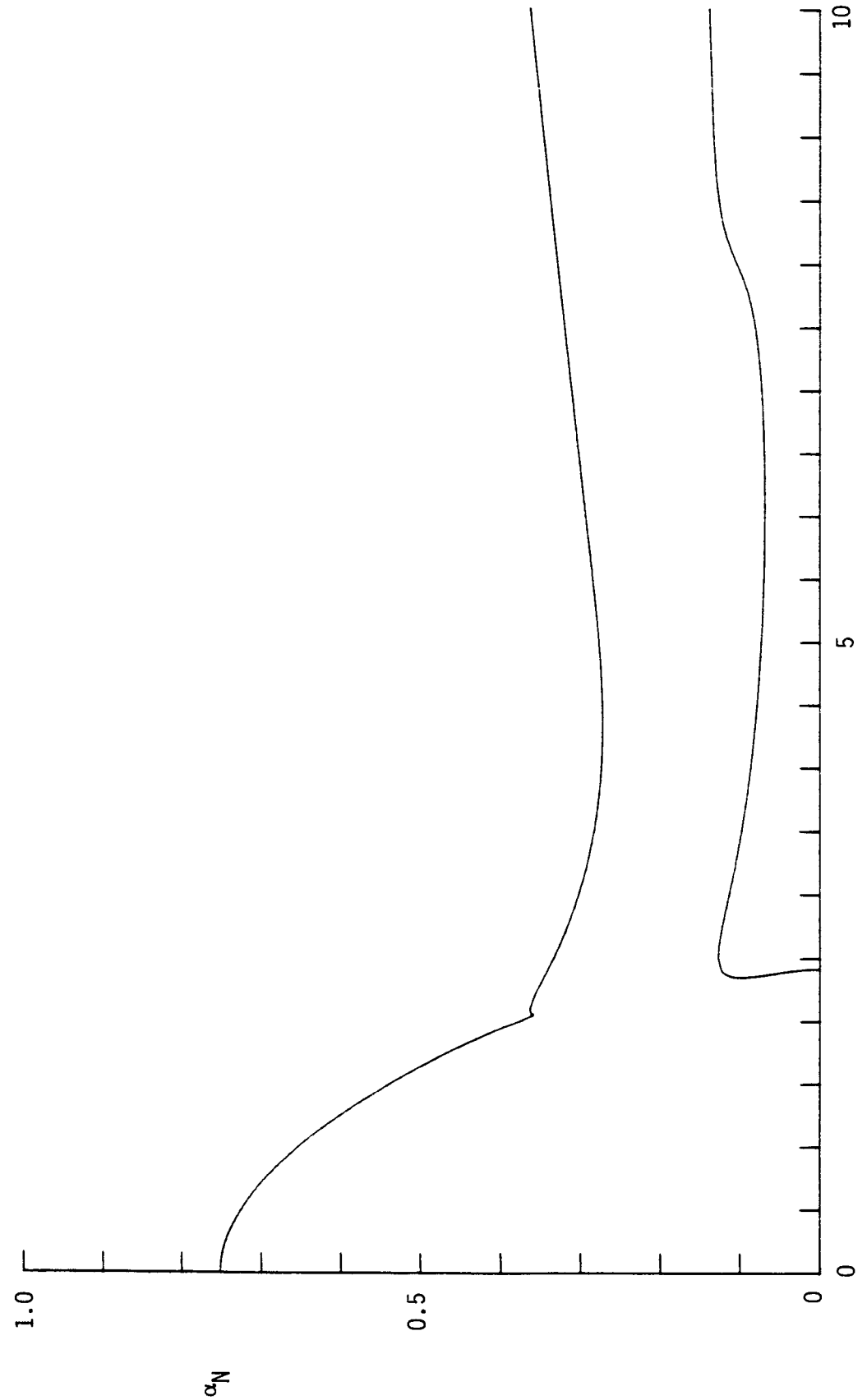

Figure 8b.

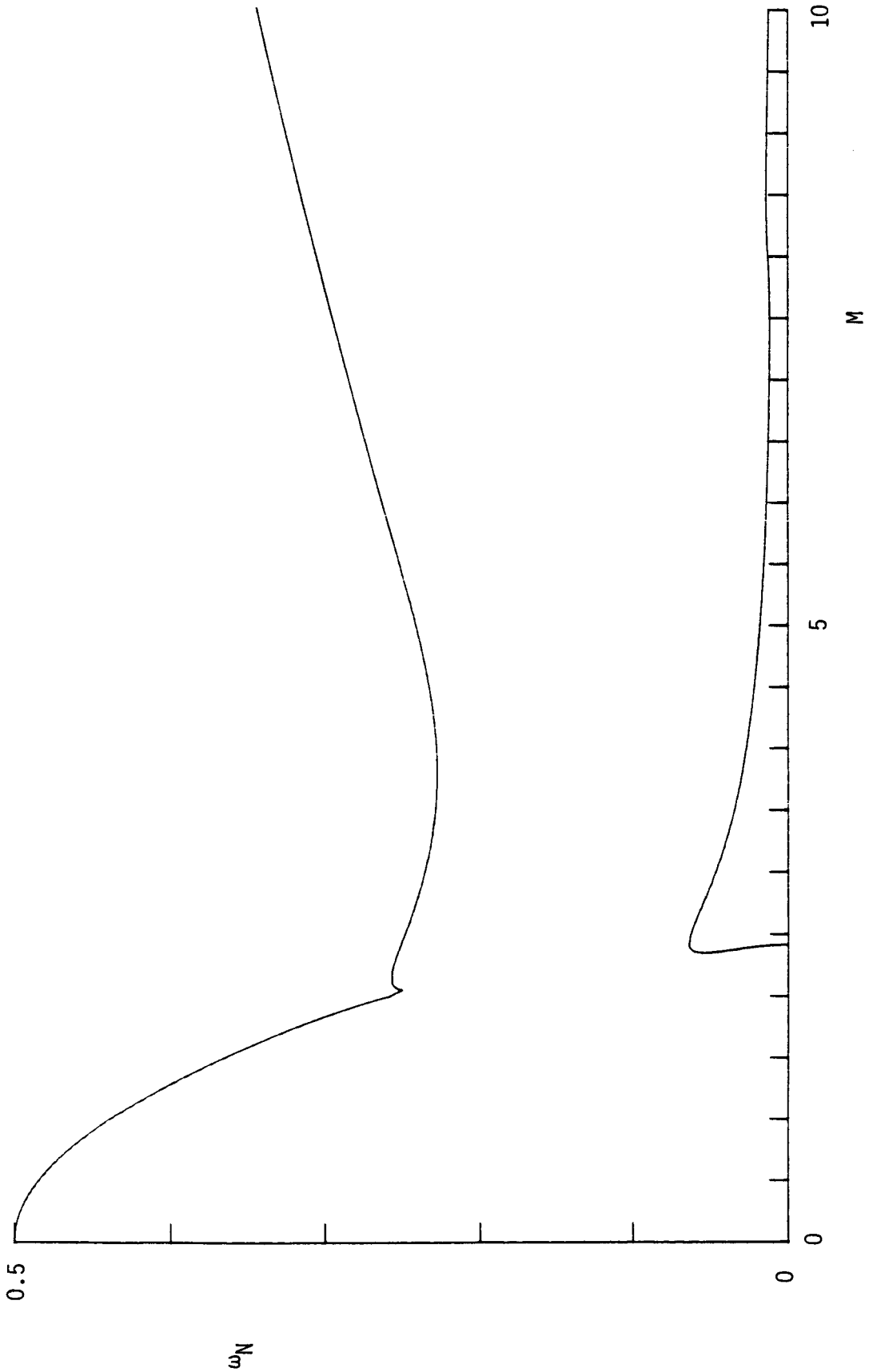

Figure 8c.

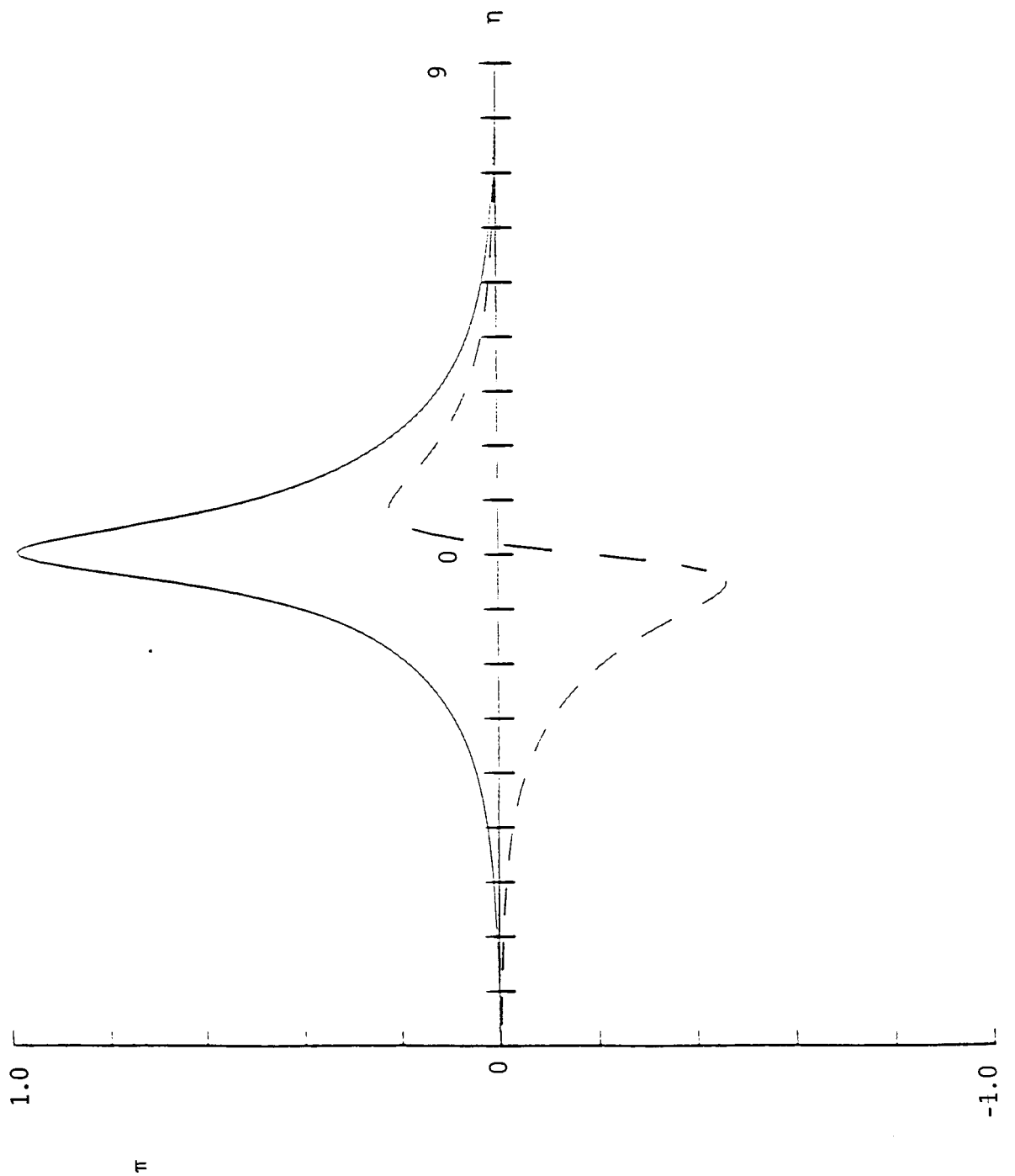

Figure 9.

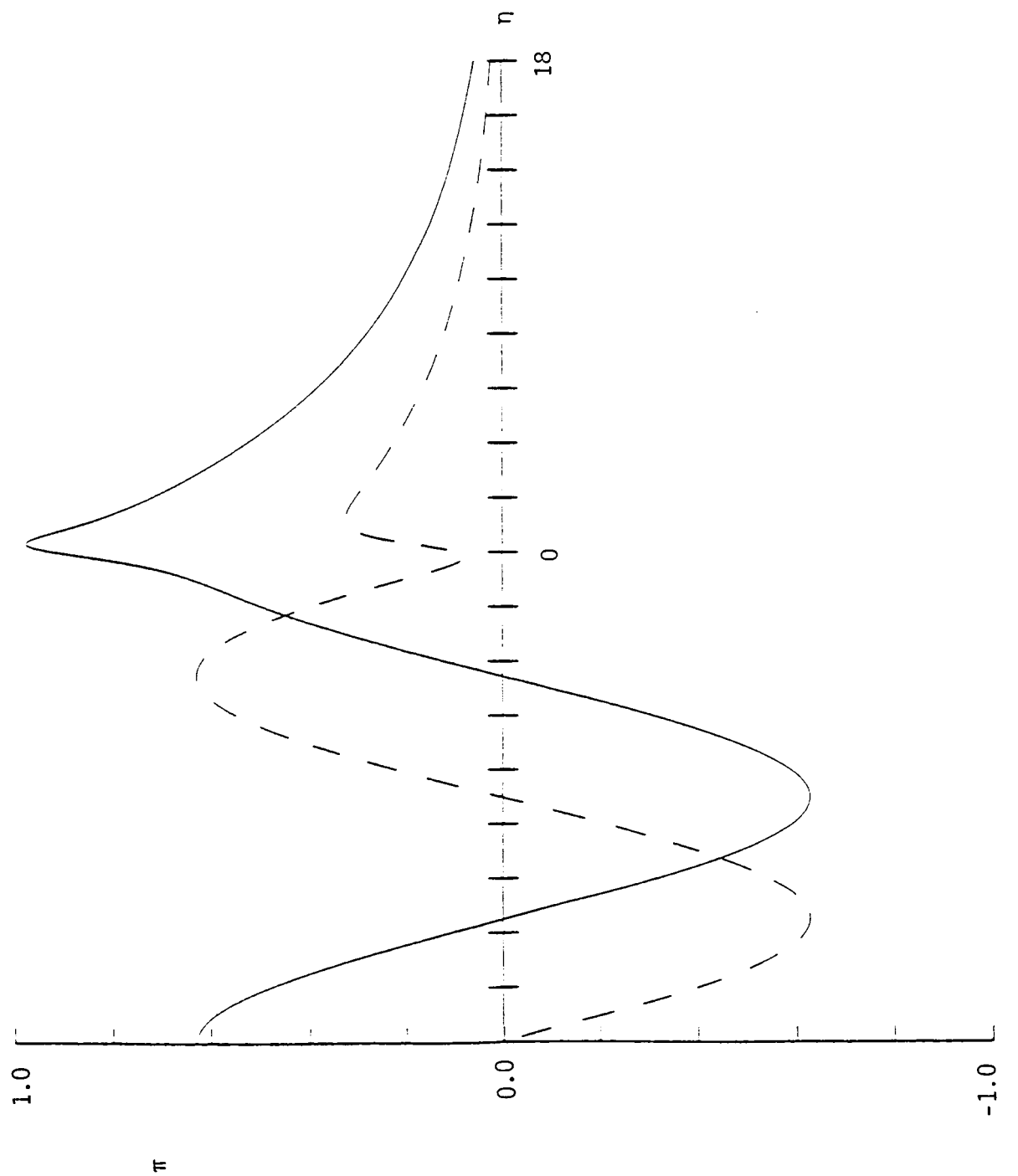

Figure 10.

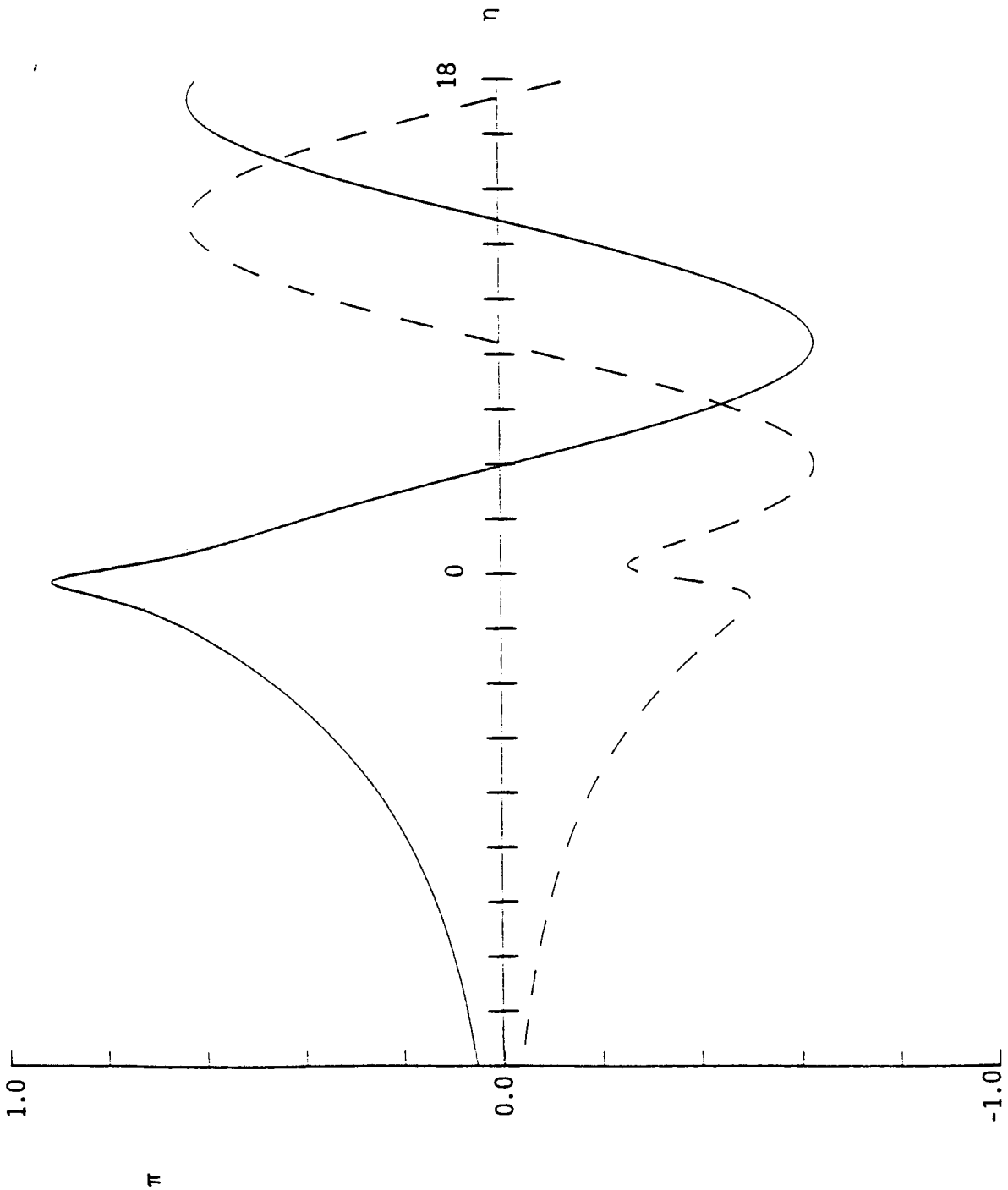

Figure 11.

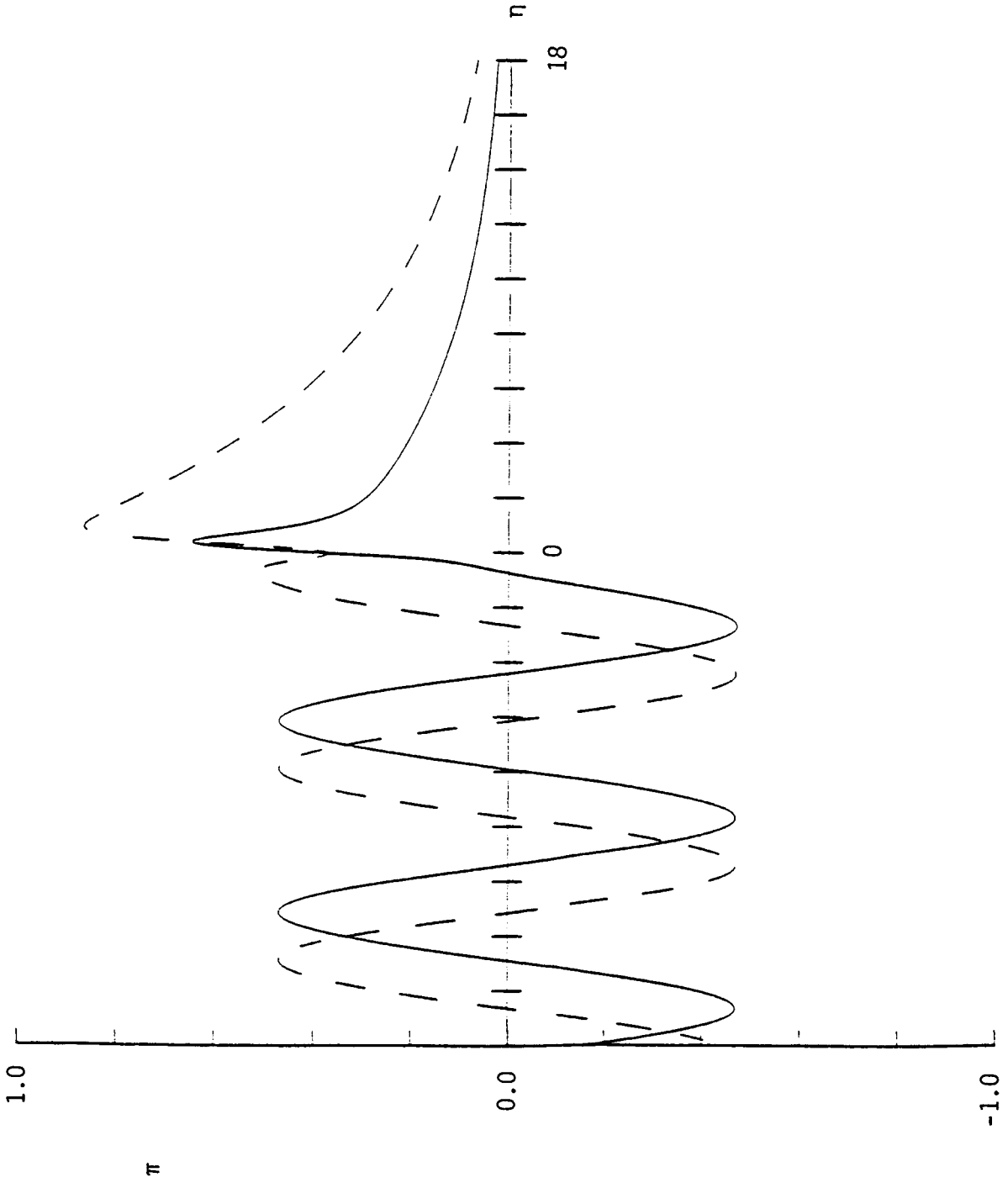

Figure 12.

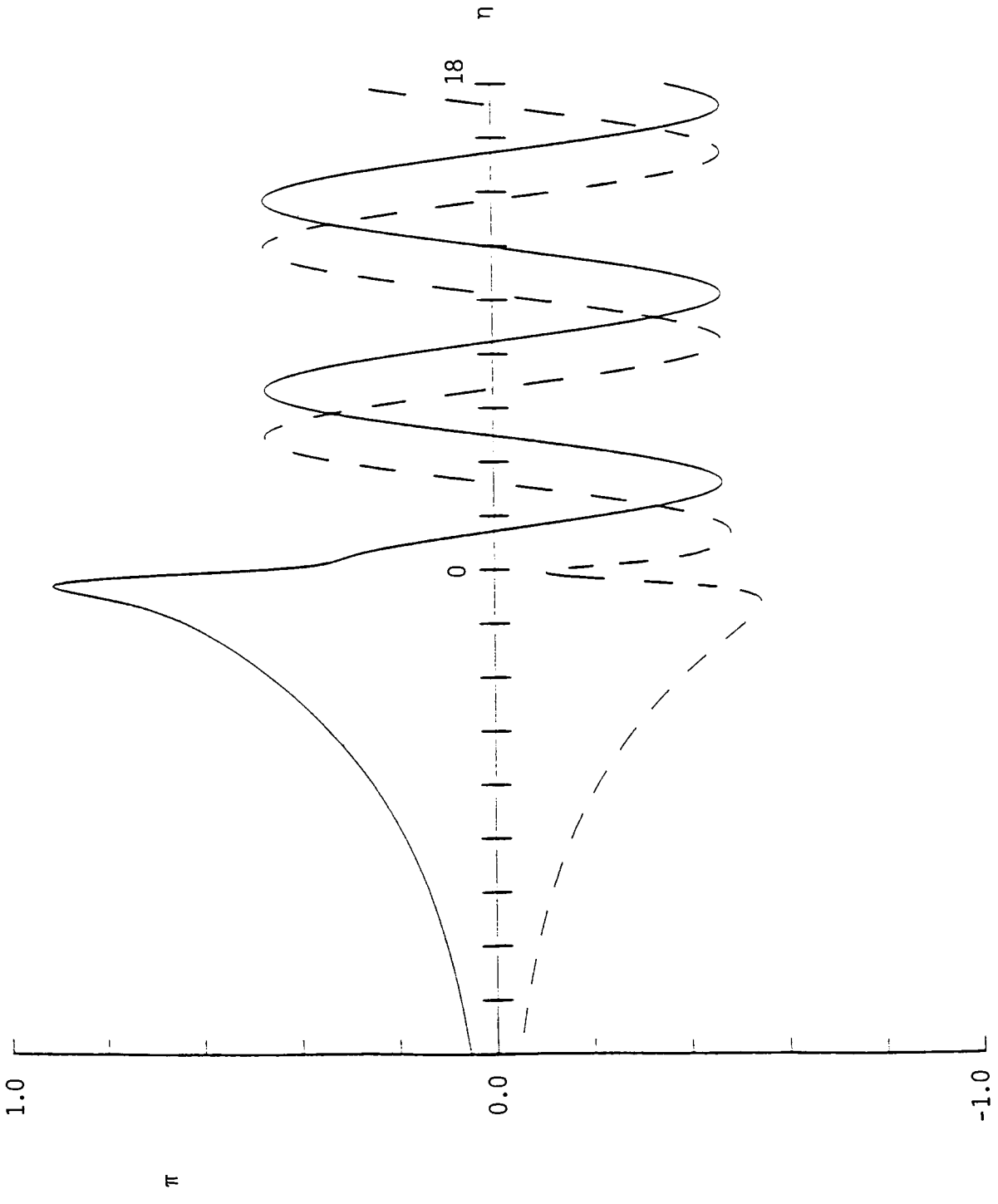

Figure 13.

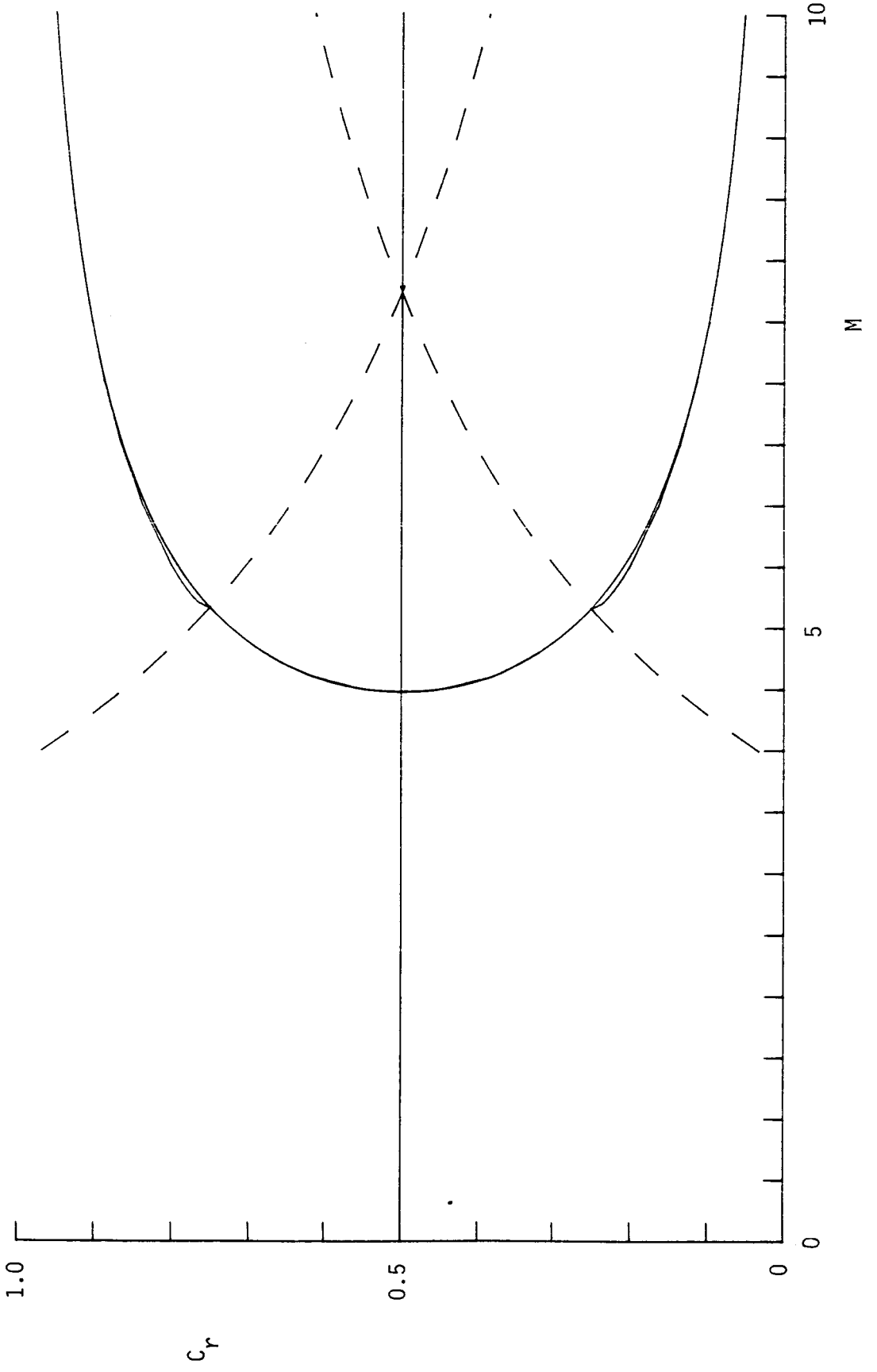

Figure 14a.

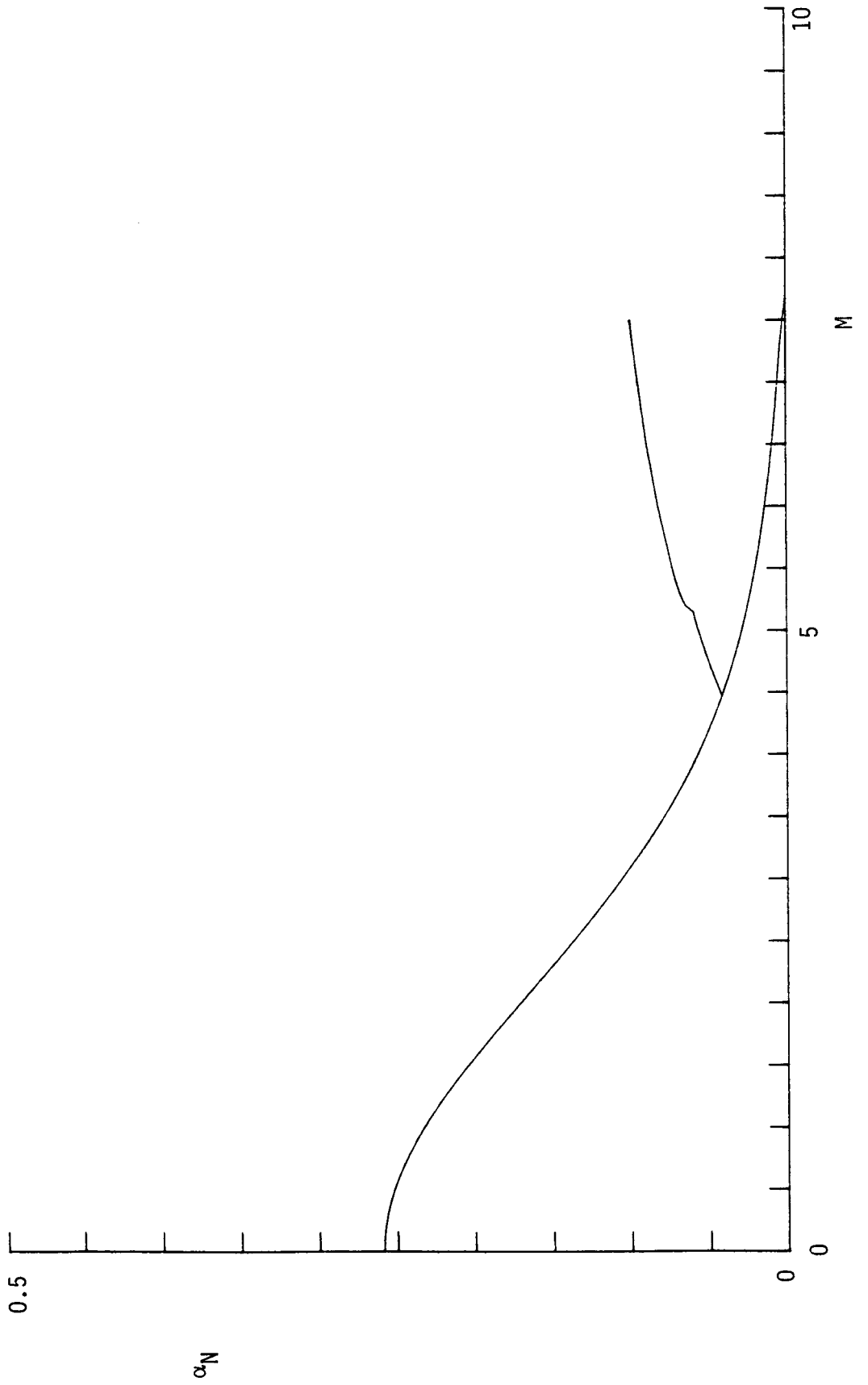

Figure 14b.

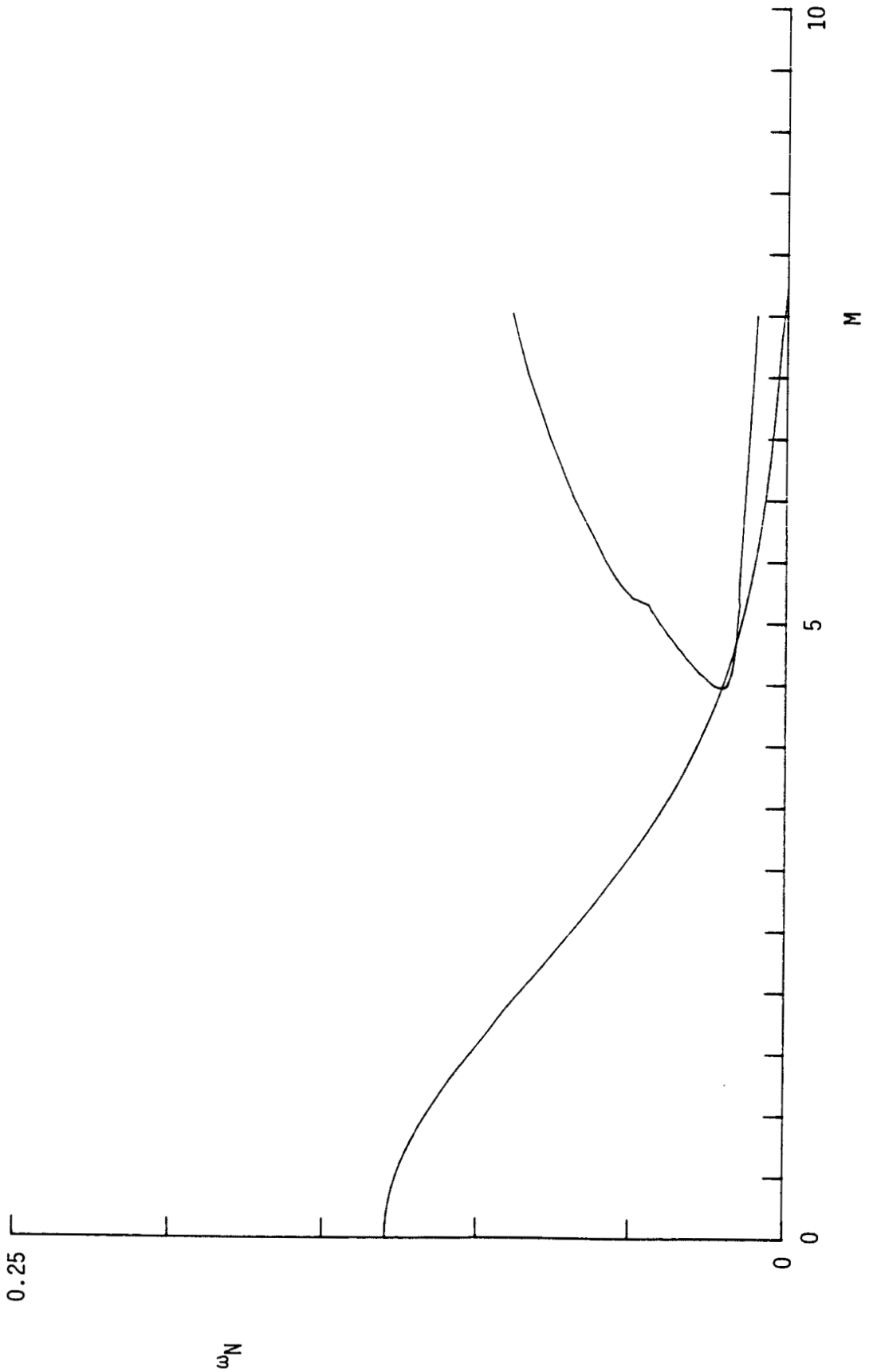

Figure 14c.

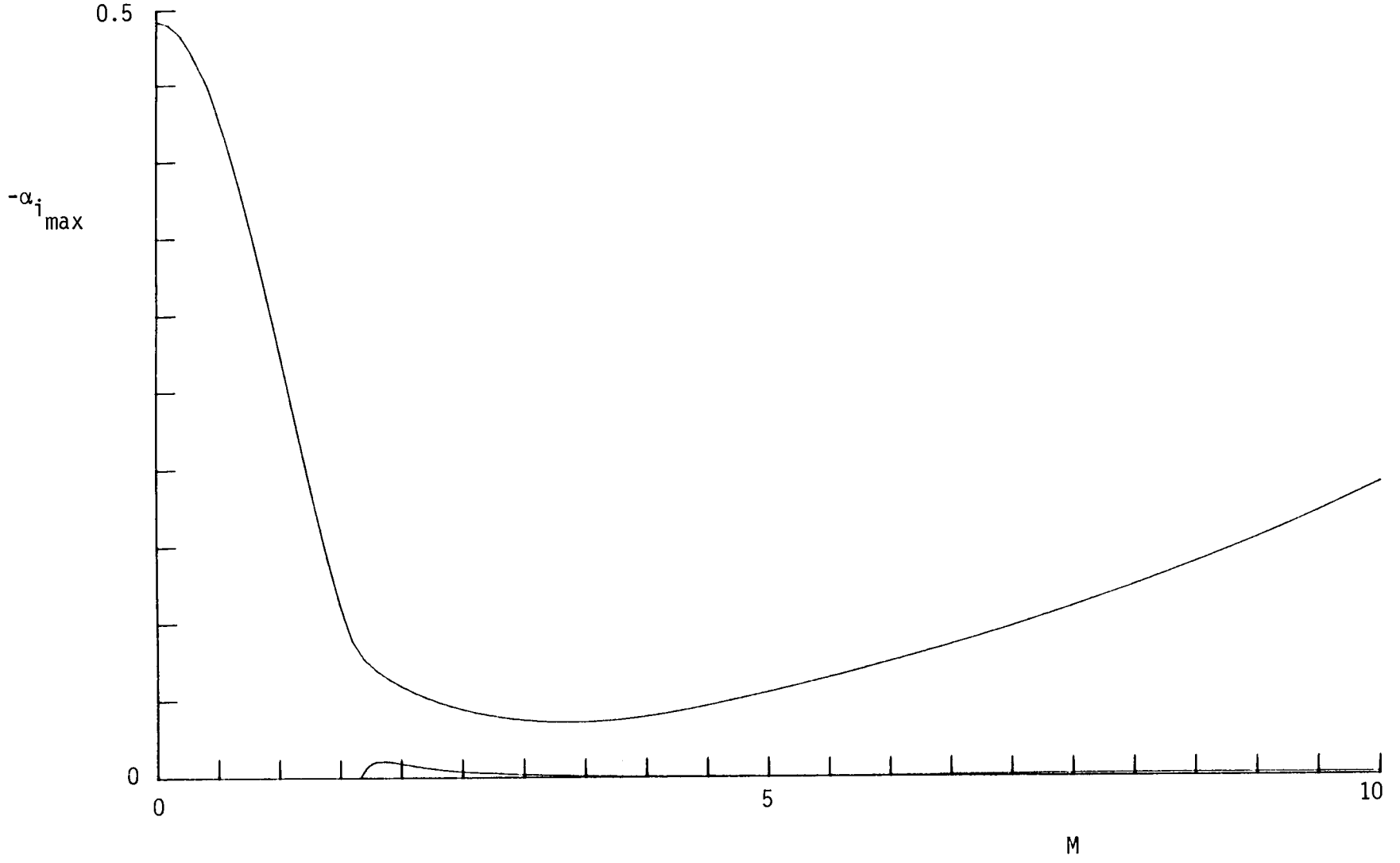

Figure 15.

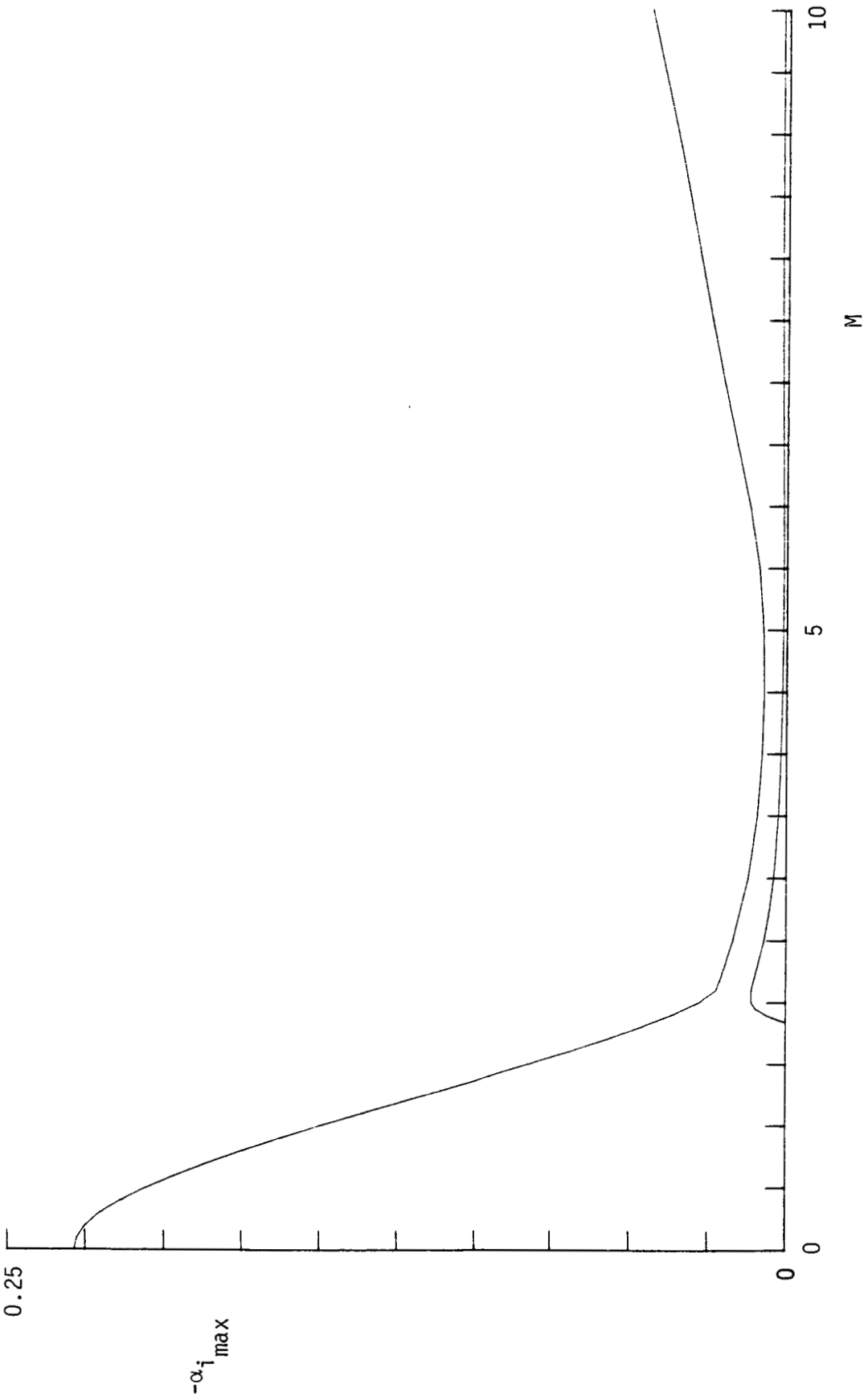

Figure 16.

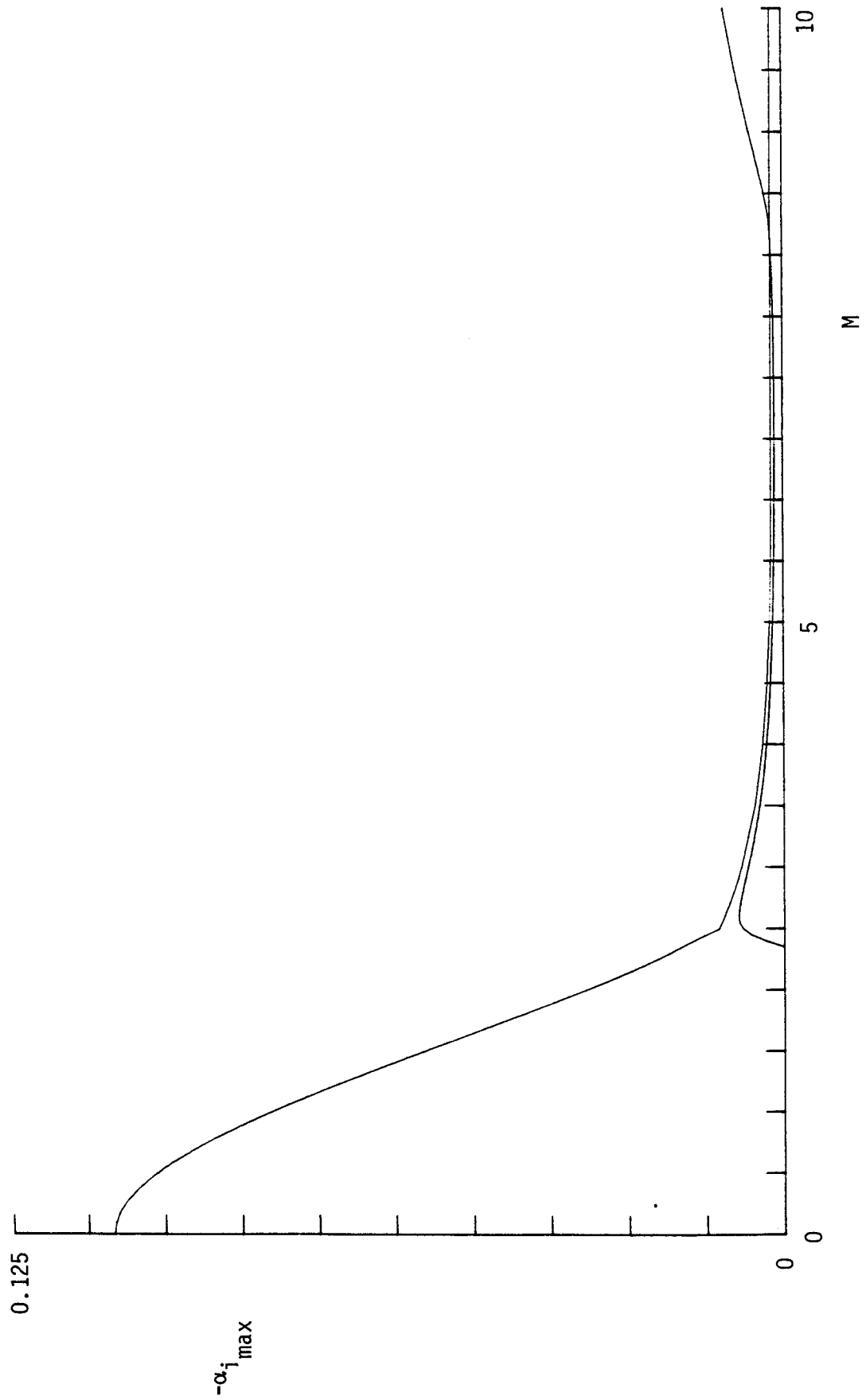

Figure 17.

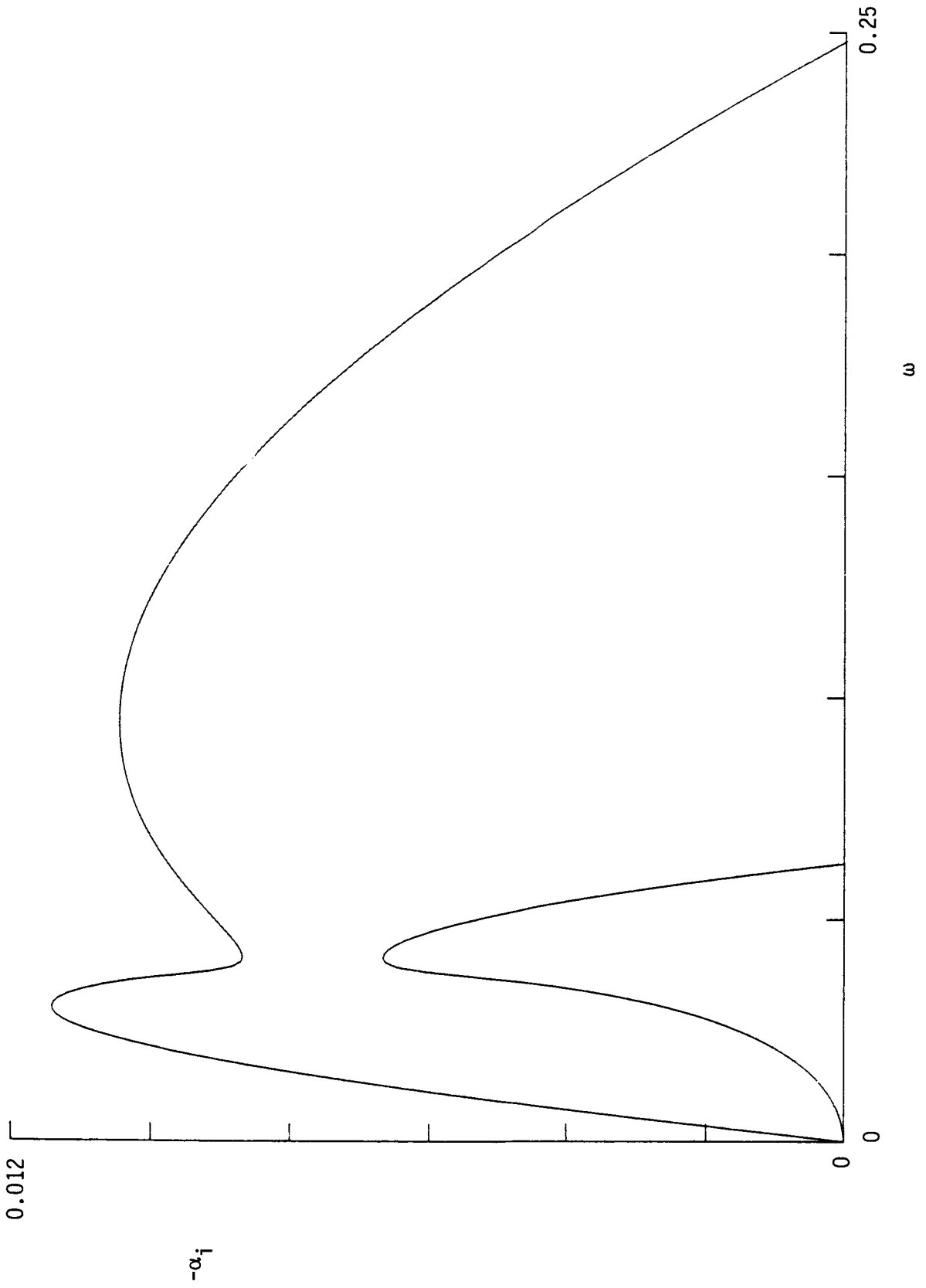

Figure 18.

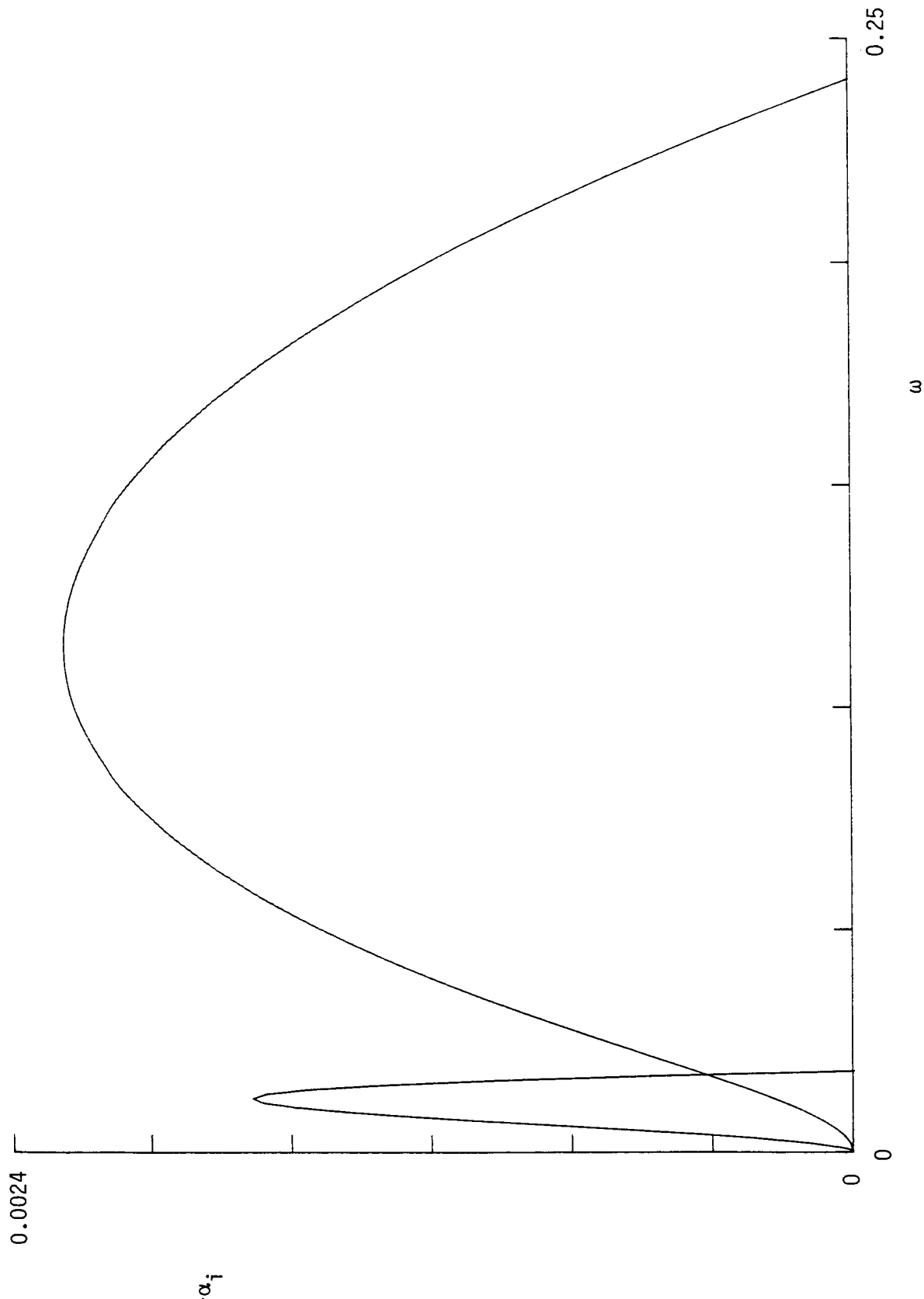

Figure 19.

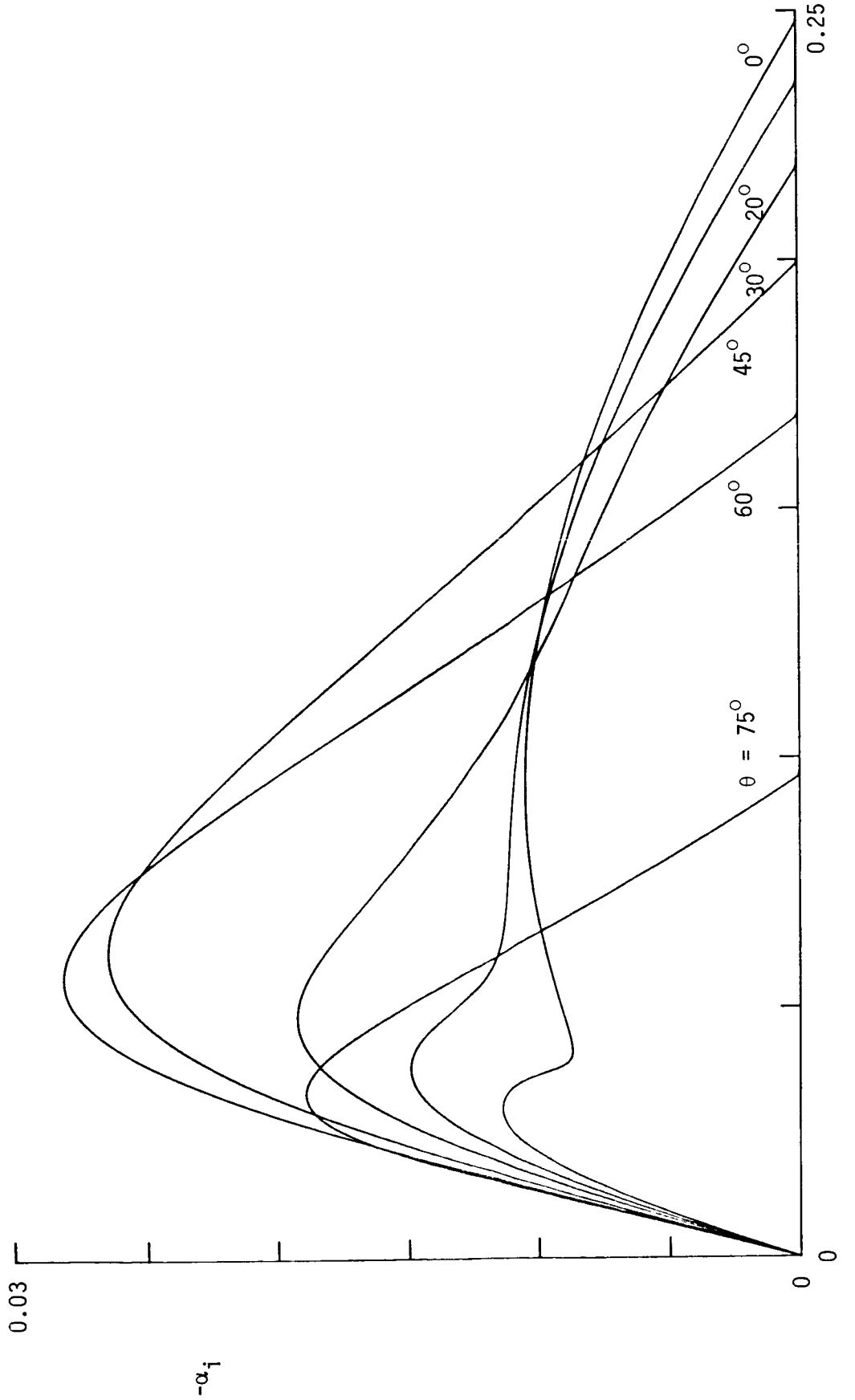
0.03
$-\alpha_i$
0
0
0.25
ω
$\theta = 75^\circ$
60°
45°
30°
20°
0°

Figure 20a.

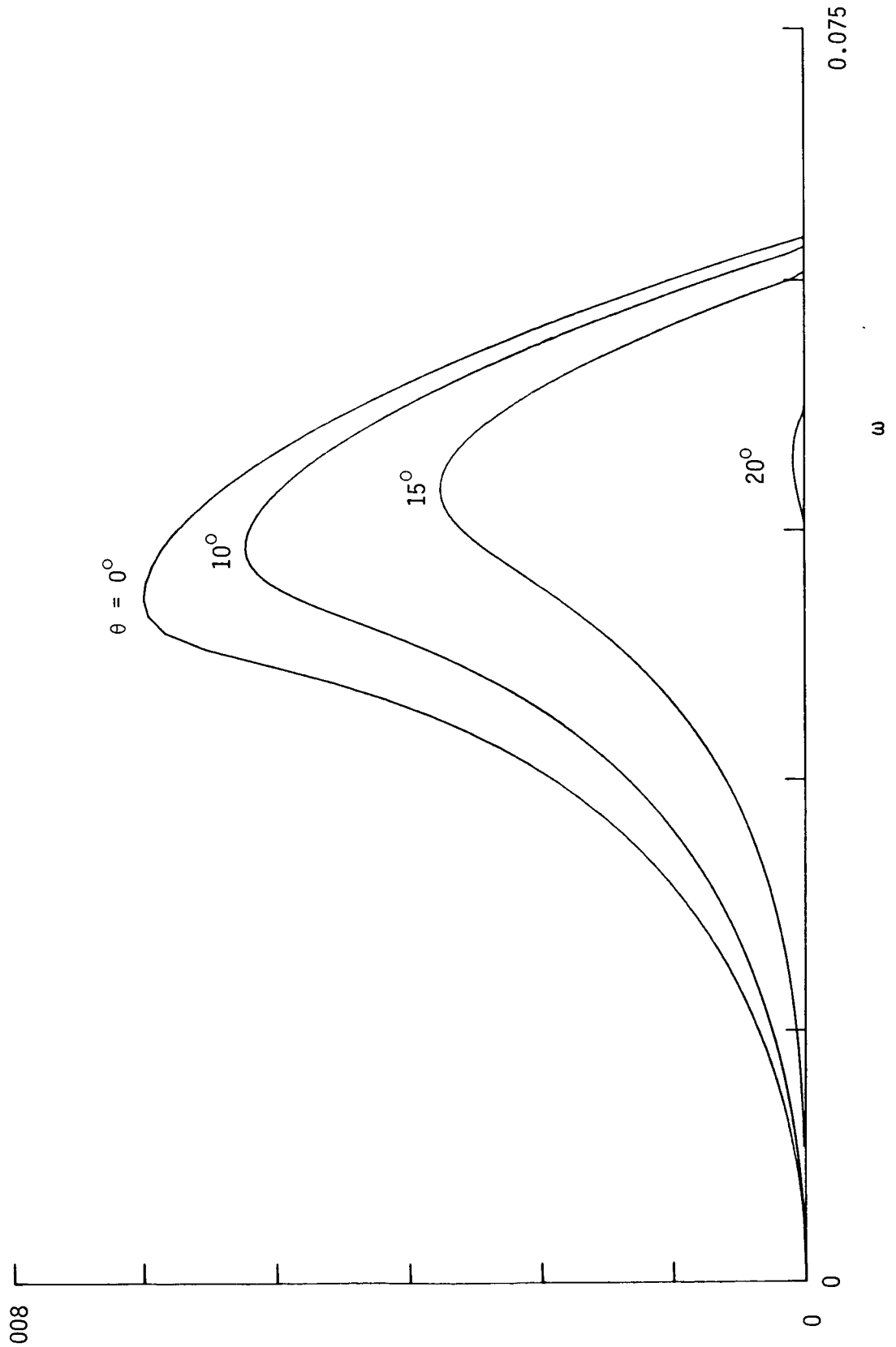

Figure 20b.

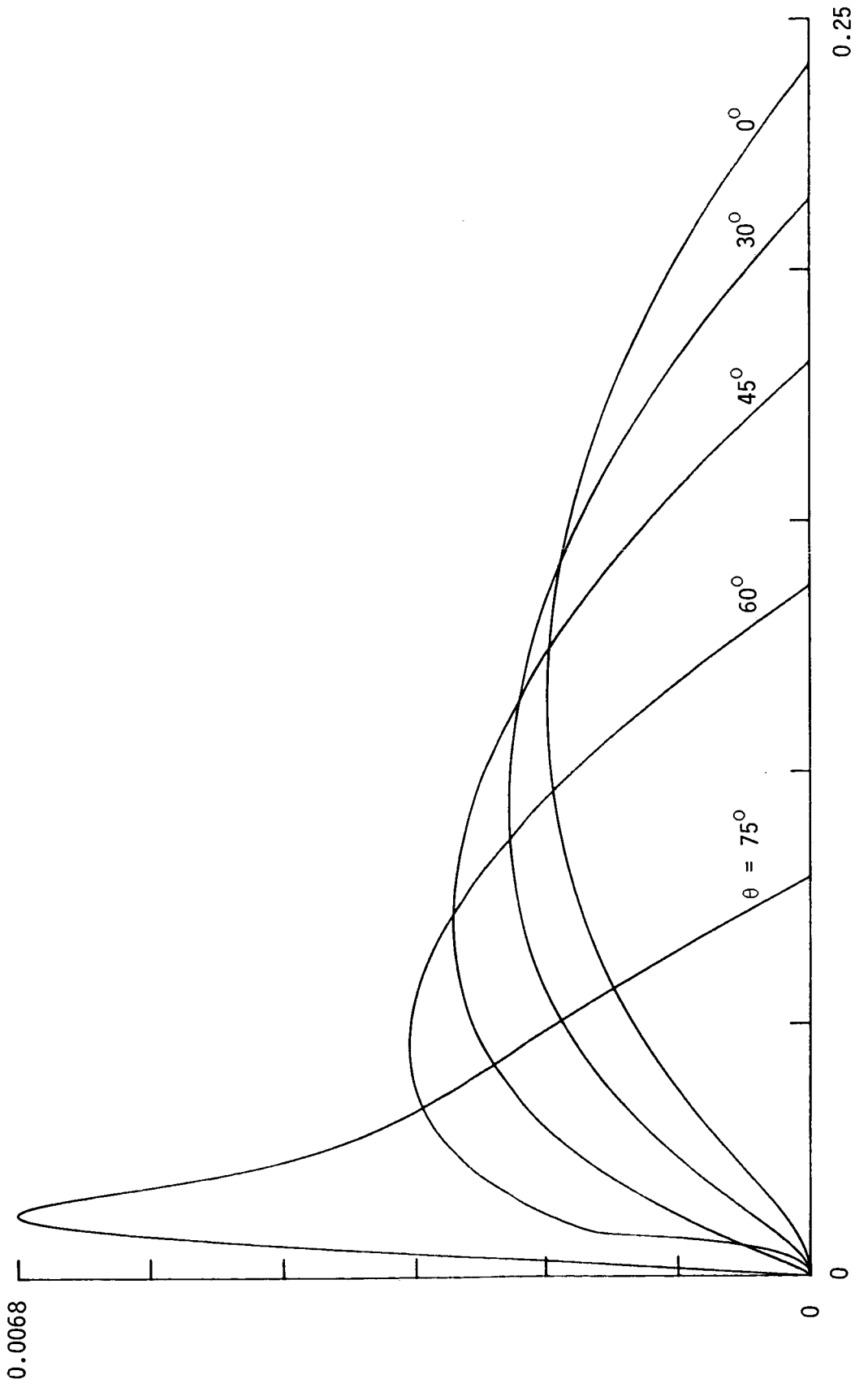
0.0068
$-\alpha_i$
0
0
0.25
ω
$\theta = 75^\circ$
60°
45°
30°
0°

Figure 21a.

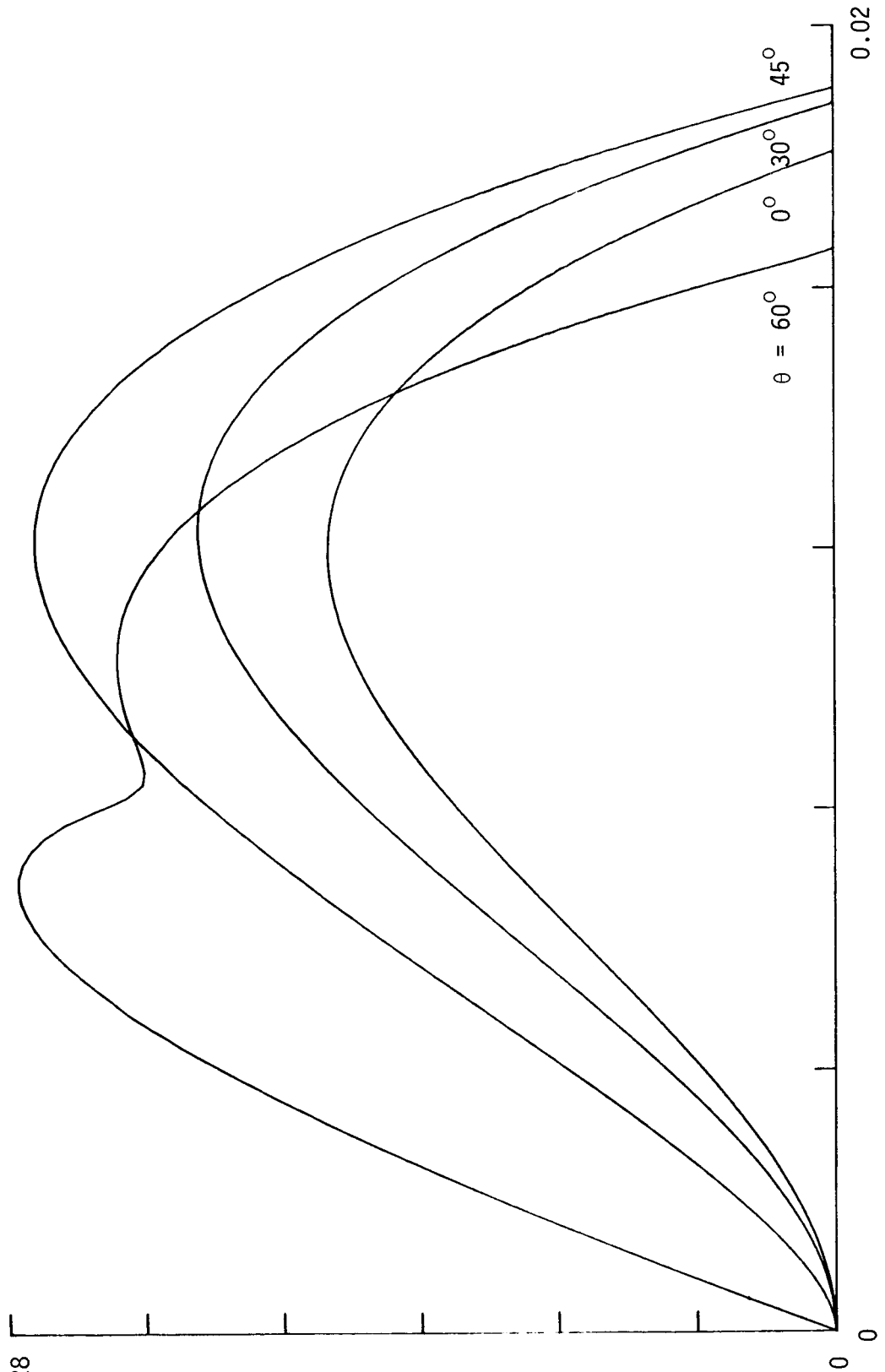

Figure 21b.

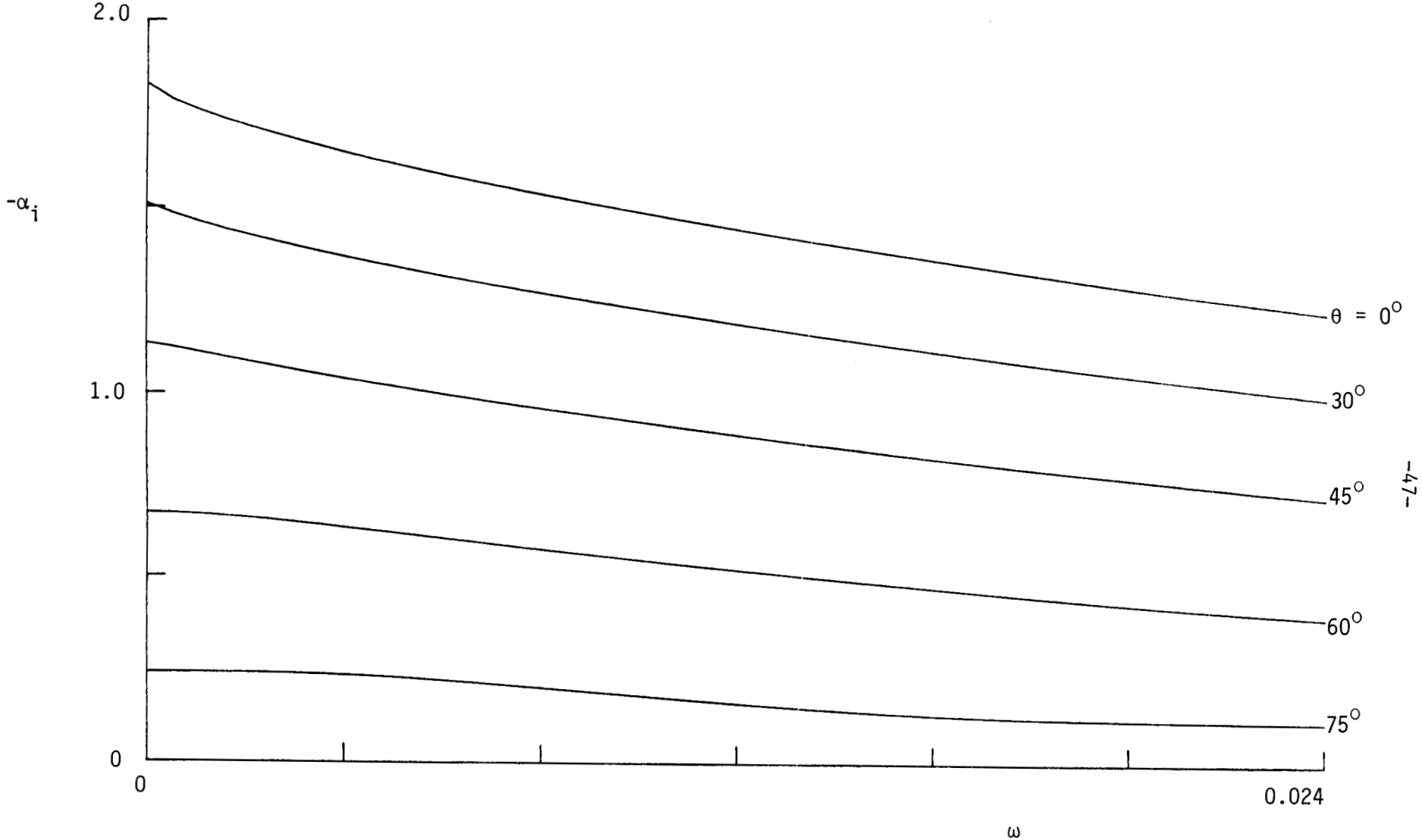
2.0
1.0
0
$-\alpha_i$
$\theta = 0^\circ$
30°
45°
60°
75°
0
0.024
ω

Figure 22.

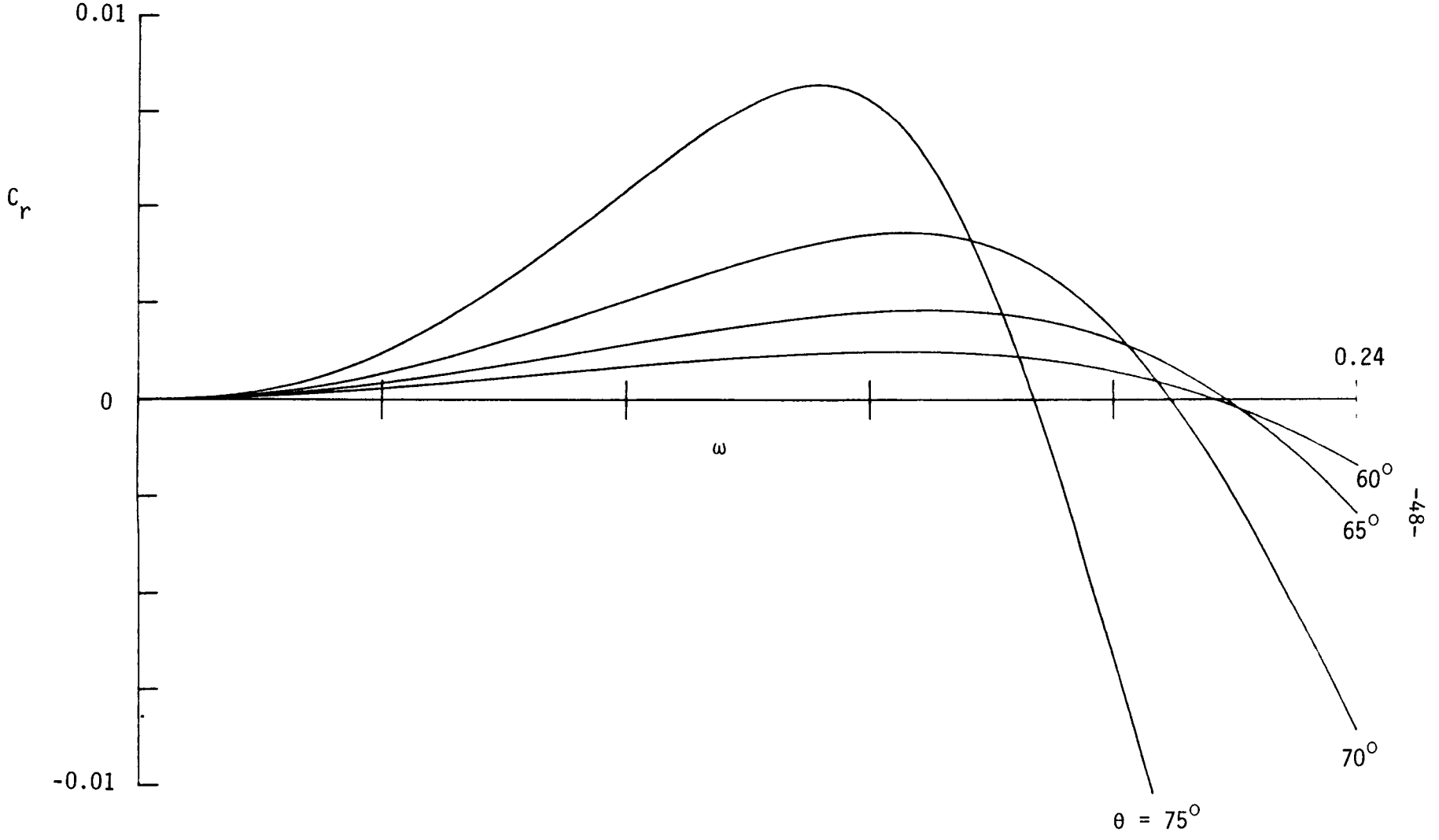

Figure 23a.

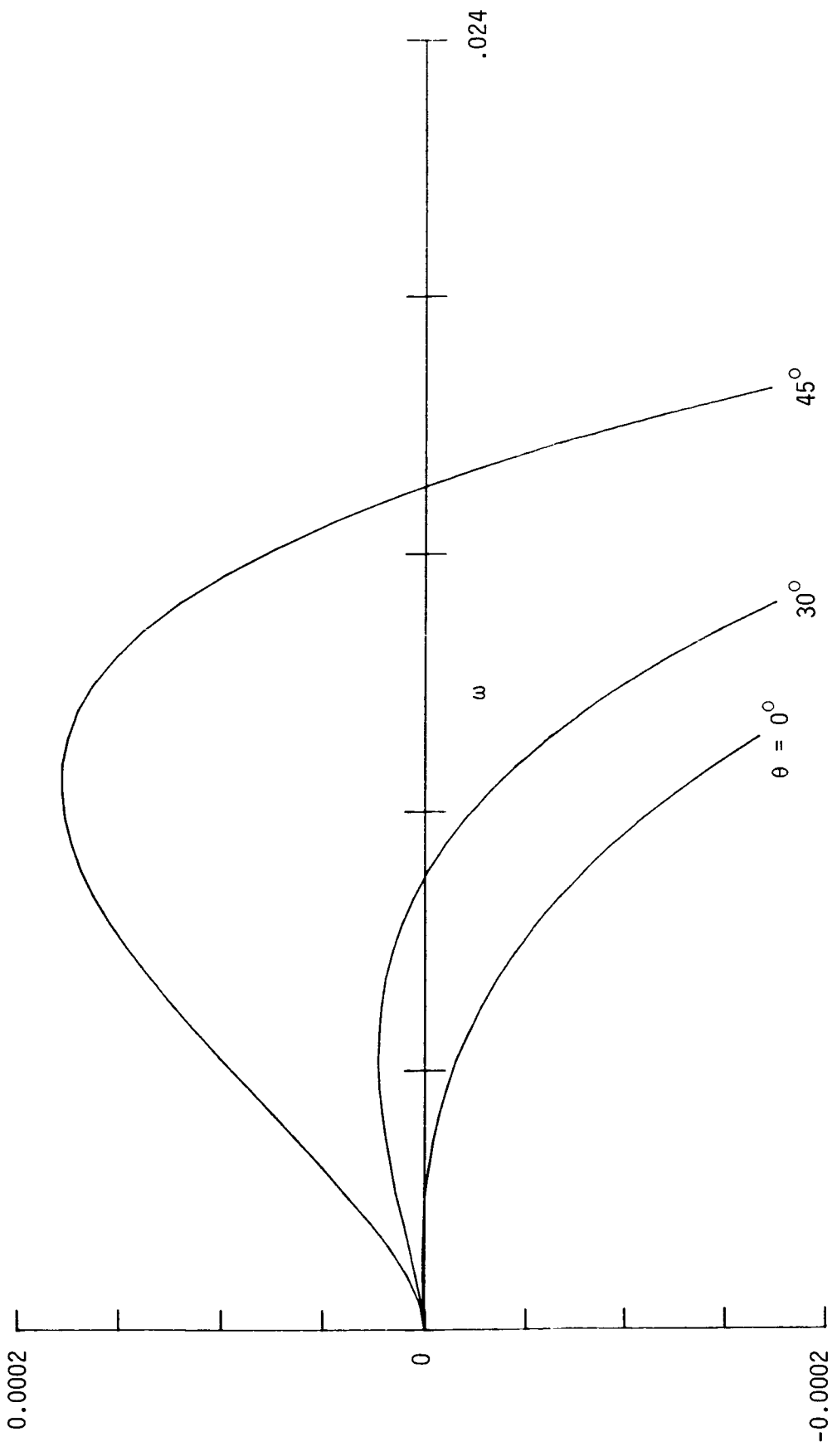

Figure 23b.

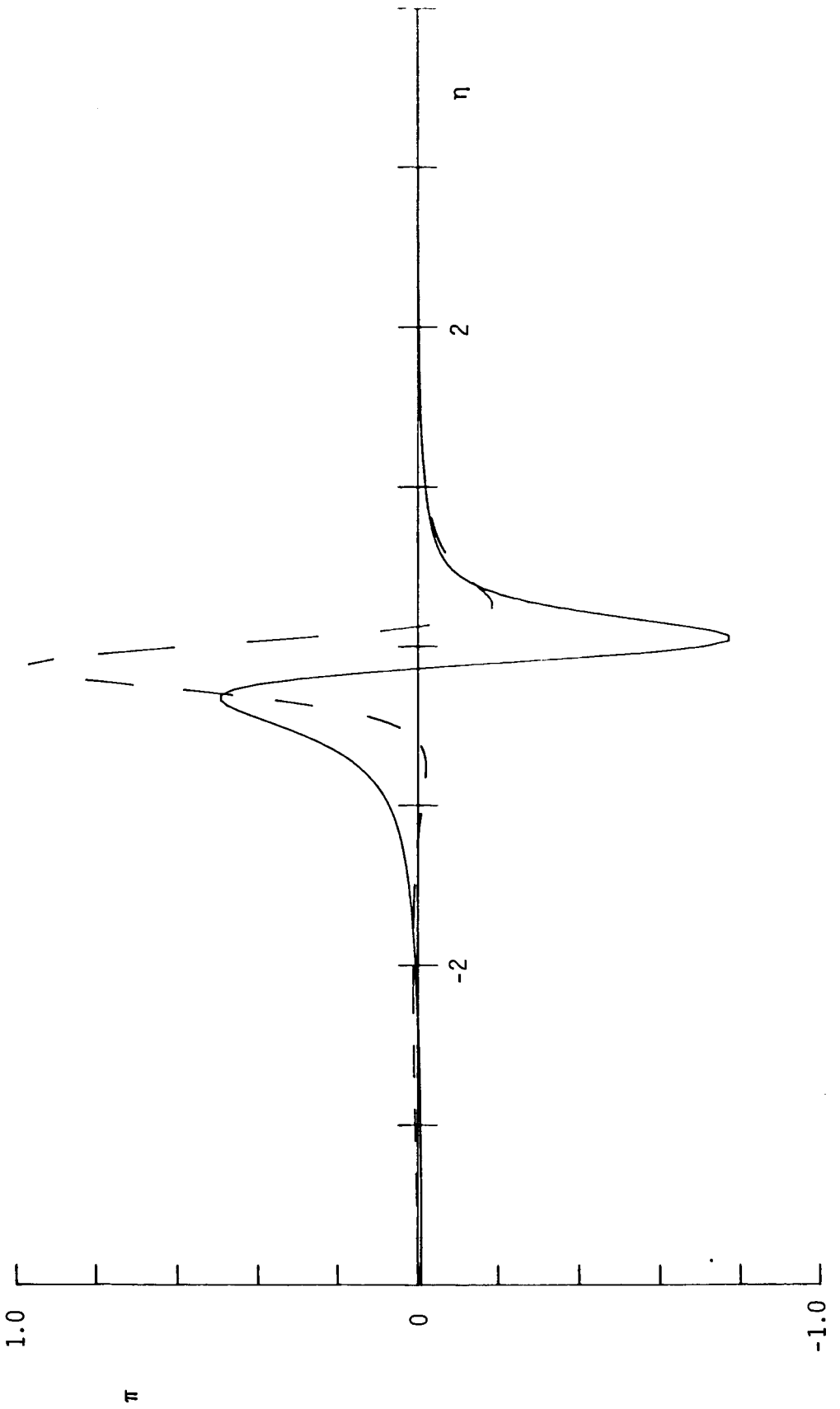

Figure 24a.

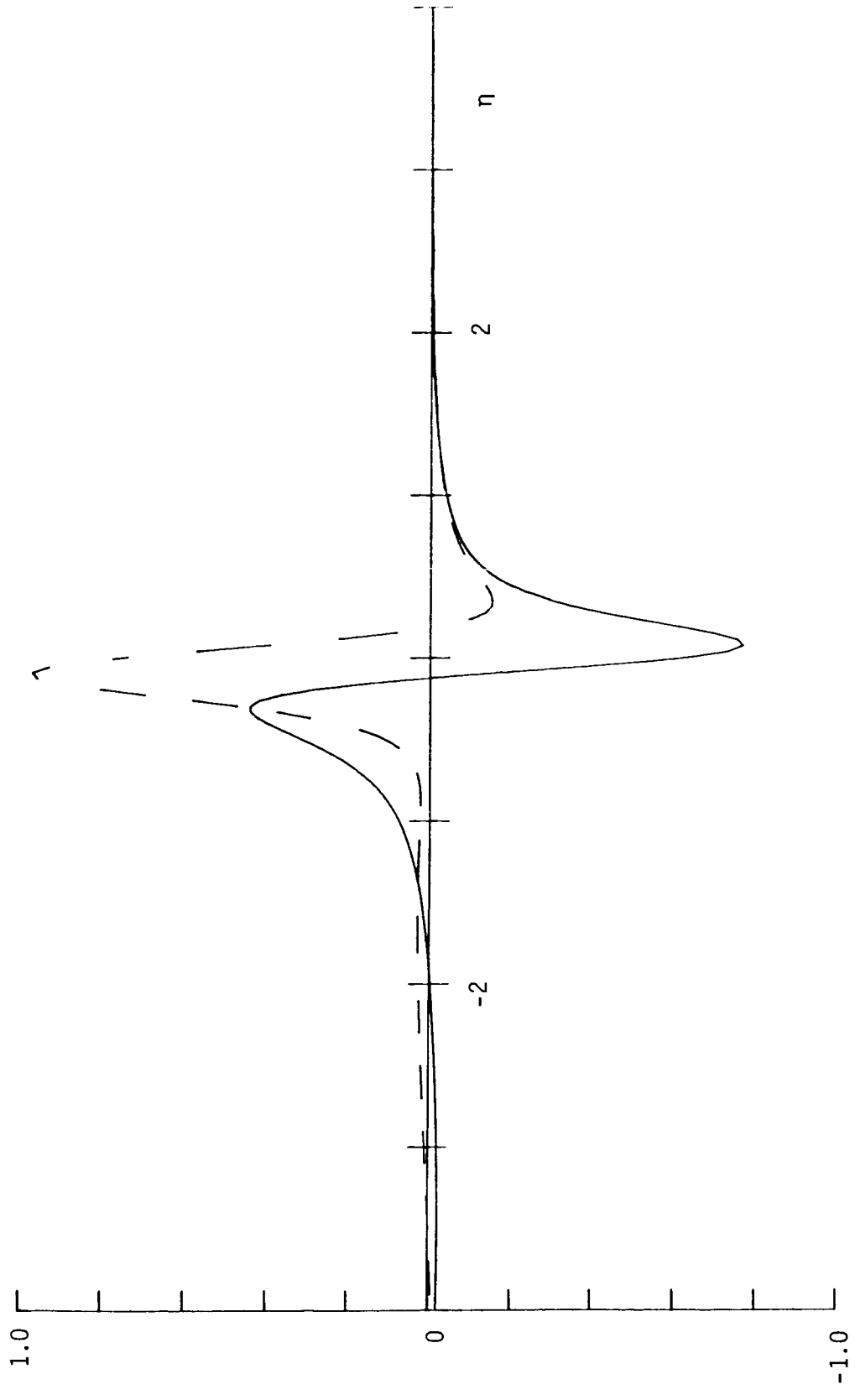

Figure 24b.

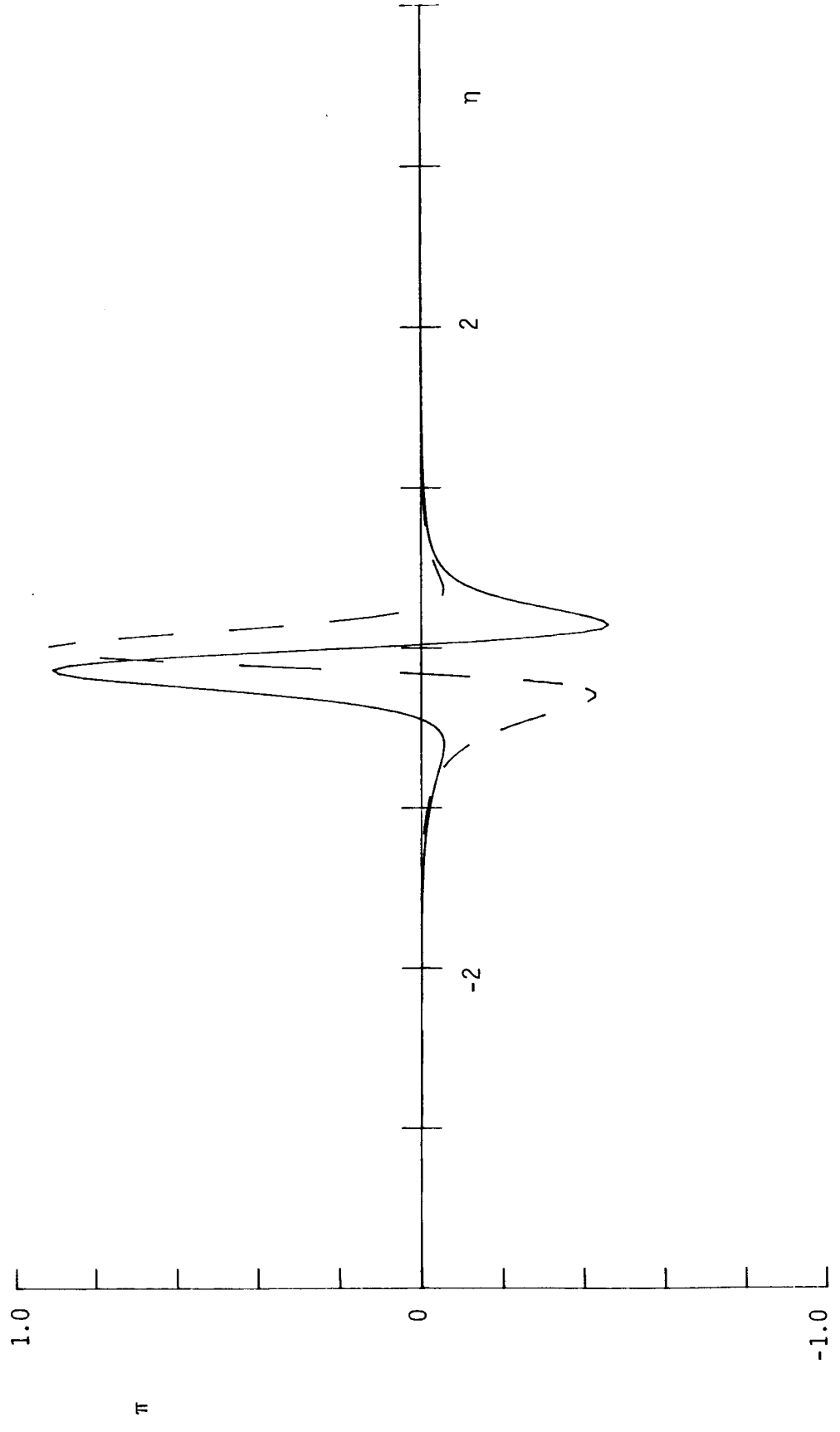

Figure 24c.

NASA
National Aeronautics and Space Administration

Report Documentation Page

1. Report No.	2. Government Accession No.	3. Recipient's Catalog No.
NASA CR-181671 ICASE Report No. 88-33		

4. Title and Subtitle	5. Report Date
SPATIAL STABILITY OF A COMPRESSIBLE MIXING LAYER	June 1988
	6. Performing Organization Code

7. Author(s)	8. Performing Organization Report No.
T. L. Jackson and C. E. Grosch	88-33
	10. Work Unit No. 505-90-21-01

9. Performing Organization Name and Address	11. Contract or Grant No.
Institute for Computer Applications in Science and Engineering Mail Stop 132C, NASA Langley Research Center Hampton, VA 23665-5225	NAS1-18107
	13. Type of Report and Period Covered Contractor Report
12. Sponsoring Agency Name and Address National Aeronautics and Space Administration Langley Research Center Hampton, VA 23665-5225	14. Sponsoring Agency Code

15. Supplementary Notes

Langley Technical Monitor: Richard W. Barnwell

Final Report

Submitted to J. Fluid Mech.

16. Abstract

We present the results of a study of the inviscid spatial stability of a parallel compressible mixing layer. The parameters of this study are the Mach number of the moving stream, the ratio of the temperature of the stationary stream to that of the moving stream, the frequency and the direction of propagation of the disturbance wave. Stability characteristics of the flow as a function of these parameters are given. It is shown that if the Mach number exceeds a critical value there are always two groups of unstable waves. One of these groups is fast with phase speeds greater than 1/2, and the other is slow with phase speeds less than 1/2. Phase speeds for the neutral and unstable modes are given, as well as growth rates for the unstable modes. It is shown that three dimensional modes have the same general behavior as the two dimensional modes but with higher growth rates over some range of propagation direction. Finally, we have found for sufficiently large Mach numbers a group of very low frequency unstable modes. These modes have very low phase speeds but large growth rates.

17. Key Words (Suggested by Author(s))	18. Distribution Statement
spatial stability, mixing layer, compressible, high Mach	34 - Fluid Mechanics and Heat Transfer 59 - Mathematical and Computer Sciences (General) Unclassified - unlimited

19. Security Classif. (of this report)	20. Security Classif. (of this page)	21. No. of pages	22. Price
Unclassified	Unclassified	54	A04